

UNIVERSIDAD DE LOS ANDES

THESIS

---

# Two-Photon Imaging Using Tunable Spatial Correlations

---

*Author:*

Juan VARGAS

*Supervisor:*

Dr. Alejandra  
VALENCIA

*A thesis submitted in fulfillment of the requirements  
for the degree of Physicist*

*in the*

Quantum Optics  
Physics Department



May 17, 2018

# Declaration of Authorship

I, Juan VARGAS, declare that this thesis titled, "Two-Photon Imaging Using Tunable Spatial Correlations" and the work presented in it are my own. I confirm that:

- This work was done wholly or mainly while in candidature for a research degree at this University.
- Where any part of this thesis has previously been submitted for a degree or any other qualification at this University or any other institution, this has been clearly stated.
- Where I have consulted the published work of others, this is always clearly attributed.
- Where I have quoted from the work of others, the source is always given. With the exception of such quotations, this thesis is entirely my own work.
- I have acknowledged all main sources of help.
- Where the thesis is based on work done by myself jointly with others, I have made clear exactly what was done by others and what I have contributed myself.

Signed:

---

Date:

---

*“I think I can safely say that nobody understands quantum mechanics”*

Richard Feynman

UNIVERSIDAD DE LOS ANDES

## *Abstract*

Science Faculty  
Physics Department

Physicist

### **Two-Photon Imaging Using Tunable Spatial Correlations**

by Juan VARGAS

Two-photon imaging is a technique for obtaining an image of an object by means of the coincidence counts of two spatially separated detectors, the first realization was reported by Pittman et al.[1]. Traditionally we need to face a single camera (detector) to the object we would like to take an image from, but with Two-photon imaging technique we obtain the image by measuring the correlations between light beams. We use a light generated by the Spontaneous Parametric Down Conversion. The popularity of this source of paired photons is strongly related to the relative simplicity of its experimental realisation, and to the variety of quantum features that down converted photons can exhibit.

We focus a 405nm CW laser to a BBO Cristal, this type-II crystal generates pairs of strongly correlated photons in a noncollinear configuration. As seen in [2], it is possible to change the spatial correlations by changing the pump waist that hits the crystal. We are interested in observing the effect on the generated images when changing the spatial correlations, these effects have to be understood as resolution of the image and the flips of the images with respect to the original object. The Two-photon imaging have some peculiar features: it is non-local; its imaging resolution differs from that of classical. These features may turn a local ‘bucket’ sensor into a nonlocal imaging camera with classically unachievable imaging resolution [3].

UNIVERSIDAD DE LOS ANDES

# *Abstract*

Science Faculty  
Physics Department

Physicist

## **Two-Photon Imaging Using Tunable Spatial Correlations**

by Juan VARGAS

Two-photon imaging es una técnica para obtener una imagen de un objeto mediante el conteo de las coincidencias de dos detectores que se encuentran espacialmente separados, la primera realización fue reportada por Pittman et al.[1]. Tradicionalmente necesitamos enfrentar una sola cámara (detector) a el objeto del cual queremos recuperar una imagen, pero con la técnica de Two-photon imaging nosotros obtenemos la imagen midiendo las correlaciones entre rayos de luz. Usamos la luz generada por el proceso de Spontaneous Parametric Down Conversion. La popularidad de esta fuente de pares de fotones esta fuertemente ligada a la relativa simplicidad de su realización experimental, y a la variedad de características cuánticas que los pares producidos pueden exhibir. Nosotros concentraremos un laser de onda continua a 405nm a el cristal BBO, este cristal tipo-II genera pares de fotones que están fuertemente correlacionados en una configuración nocolineal. Como visto en [2], es posible cambiar las correlaciones espaciales cambiando la cintura del bombeo que llega a el cristal. Estamos interesados en observar el efecto en las imágenes generadas cuando cambiamos la correlación espacial, estos efectos tienen que entenderse como la resolución de la imagen y las rotaciones de las imágenes con respecto a el objeto original. El Two-photon imaging tiene algunas características peculiares: no es local; su resolución difiere a la resolución clásica. Estas características convertirían un sensor bucket en una cámara no local con resolución clásicamente inalcanzable [3]

## *Acknowledgements*

My very first thanks must go to my parents, without them and their unconditional support through this years nothing of this would be possible. I also would like to thank my brothers for being always a good example for myself.

The present monograph is the compilation of the efforts of many people, First of all I would like to thank director Alejandra Valencia, for showing me a different perspective about experimental physics and for the many discussions we had where I've learnt a wide set of things. There must be also a special thanks to the Quantum Optics group. To Omar Calderon for sharing the theoretical and experimental skills necessary to have a source light with Tunable spatial correlations. To Daniel Urrego and Johnny Tenorio for instruct me in most of the experimental procedures and to Juan Andrés Urrea for the numerical solutions used in this monograph.

# Contents

<b>Declaration of Authorship</b>	<b>i</b>
<b>Abstract</b>	<b>iii</b>
<b>Acknowledgements</b>	<b>v</b>
<b>1 Introduction</b>	<b>1</b>
<b>2 Theory</b>	<b>4</b>
2.1 Correlations between two photons . . . . .	4
2.1.1 Spontaneous Parametric Down Conversion . . . . .	5
2.1.1.1 Phase matching conditions . . . . .	6
2.1.2 Spatial Correlations . . . . .	7
2.1.3 Tunable Spatial Correlation SPDC source light . . . . .	10
2.2 Imaging . . . . .	10
2.2.1 Standar Imaging . . . . .	11
2.2.2 Two-photon Imaging . . . . .	13
2.2.2.1 LenslessTwo-photon Imaging using entangled photon . . . . .	14
2.2.2.2 Effect of the different spatial correlations . . . . .	17
<b>3 Experimental Setup</b>	<b>19</b>
3.1 Light Source with Tunable Spatial Correlations . . . . .	19
3.1.1 Spatial Filter to achieve a Gaussian pump beam . . . . .	20
3.1.2 Lenses to Control the pump beam waist . . . . .	21
3.1.3 BBO(Beta Barium Borate) Crystal: The source of pair of photons . . . . .	23
3.2 Spatial Correlations Measurement Setup . . . . .	23
3.2.1 Detection Module . . . . .	25
3.2.2 Single Photon Counting Module(SPCM) . . . . .	26
3.2.3 Field-programmable gate array(FPGA) . . . . .	26
3.2.4 Computer(Data Analysis) . . . . .	26
3.3 Two-Photon Imaging Setup . . . . .	27

<b>4 Results</b>	<b>29</b>
4.1 Achiving a Gaussian Beam . . . . .	29
4.2 Finding The Correlated Photons . . . . .	30
4.3 Experimental Correlations . . . . .	31
4.4 Mask Alignment . . . . .	32
4.4.1 Alignment Mask 1 . . . . .	32
4.4.2 Alignment Mask 2 . . . . .	32
4.4.3 Alignment Mask 3 . . . . .	33
4.5 Two-Photon Images . . . . .	34
4.5.1 Two-photon imaging Mask 1 . . . . .	35
4.5.2 Two-photon imaging Mask 2 . . . . .	35
4.5.3 Two-photon imaging Mask 3 . . . . .	35
<b>5 Discussions and Conclusion</b>	<b>37</b>
<b>A Two-photon Imaging Using Chaotic Sources</b>	<b>39</b>
<b>Bibliography</b>	<b>42</b>

# List of Figures

1.1	Eye seen as a Optical System, where $d$ is the distance between object and OS . . . . .	1
1.2	Two-photon imaging techniche setup . . . . .	2
2.1	Simple Experimental setup for the type-II noncollinear SPDC process . . . . .	5
2.2	Theoretical Spatial correlations between a pair of down-converted photons, $w_p = 91\mu m$ . . . . .	8
2.3	Positive and Negative ideal spatial correlations . . . . .	9
2.4	Simulated correlations $w_p = 15\mu m$ . . . . .	10
2.5	Optical imaging: a lens produces an image on an object at $S_i$ . This distance is defined by the Gaussian thin-lens equation . . . . .	11
2.6	sombrero-like function behaviour for differents constants . . . . .	12
2.7	Simple schematic for the Two-photon Imaging. Only in the coincidence counts we can reconstruct the image . . . . .	13
2.8	Simple schematic for a Two-photon Imaging using entangled photons and a 2-f system . . . . .	15
2.9	Simulated Two-photon images for two different waist, $w_p = 15\mu m$ and $w_p = 91\mu m$ , Where $T(\vec{r}_B)$ is an square in the second quadrant. . . . .	18
3.1	Experimental Setup for the SPDC light Source . . . . .	19
3.2	The spatial intensity profile before and after the spatial filtering process , Taken from [4] . . . . .	20
3.3	The spatial intensity profile measured after the spatial filter . . . . .	21
3.4	Effect of lens on a Gaussian beam[5] . . . . .	22
3.5	Composition of lenses to control the Pump Waist at a Fixed distance $F$ . . . . .	22
3.6	Experimental Setup for Obtaining the spatial correlations of a pair of down-converted photons . . . . .	24
3.7	The plane that is being scanned by the fiber tip, it is a $4x4mm$ square, that can be scanned in N steps, where N is defined by us	25

3.8	Single Photon Counting Module	26
3.9	Experimental Setup for the Two-photon Imaging	27
3.10	Mask 1: Detailed description of the 'square' aperture location in the scanned plane	28
3.11	Mask 2: The letter 'L' pointing down. Mask 3: Opening question mark.	28
4.1	Propagation of the pump Beam, the graph shows how the $w_p$ changes with distance	30
4.2	Fit for the change in the $w_p$ with distance, at 13.5% intensity	30
4.3	(a) and (b) shows the B-photon of the down converted pair. In (b) we moved away the translational mount of the mask	31
4.4	Experimental Spatial correlations between a pair of down-converted photons. <i>XX Correlation</i> shows the correlation in the x variables, <i>YY Correlation</i> shows the correlation in the y variables, Beam propagating in the z direction. $w_p = 91\mu m$	32
4.5	Localization of the mask with an square	33
4.6	Moving the L Mask in order to put it in the most central spot	33
4.7	Long exposure of the definitive localization of the mask, in this try we leave the detector in each place for 30 seconds, we also make the steps of the detector smaller, $0.1mm$	34
4.8	Interrogation definitive position	34
4.9	Experimental Two-photon image recovered for the square aperture	35
4.10	Two-photon image recovered for the L aperture.	36
4.11	Two-Photon Image Interrogation	36
A.1	Experimental setup for the Two-photon imaging using thermal light, taken from [6]	39

# Chapter 1

## Introduction

Imaging is a process that we are doing all the time, we have a pair of optical systems (OS) that are mapping constantly, and doing a recreation of the things around us. This pair of OS is what we call eyes, without them we would be able just to *feel* what surround us, it would be impossible to *see*, to do an *image* of our surroundings. The components of the eye are a well established optical system, this OS uses the light that is reflected or scattered from the objects and then comes towards the eye. At the back of the eye, we have a photodetector that is called Retina, it converts the photons into electrical signals that travels through our Brain, where the image is then recovered. Figure 1.1 shows a really simplified schematics of the eye seen as an OS.

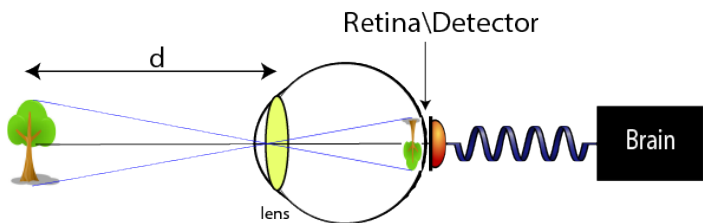


FIGURE 1.1: Eye seen as a Optical System, where  $d$  is the distance between object and OS

For taking a photograph of an object, traditionally, we need to face a camera detector for example a CCD to the object, in a way similar to what we do when we point out our eyes to the objects we are seeing, Figure 1.1. Both retina and camera record the spatial shape of the light that comes through. This spatial information is necessary then for the process of reconstructing an image of an object. It is important to point out that when using cameras we usually make images that are 2D representations, of 3D objects. For this reason we talk about an image plane, which is the plane where, depending on the OS, the 2D representation of the object is going to be formed.

What would happen if our retina or camera stopped recording the spatial shape of the light? if our retina now is only able to detect the light that

reaches it, but not where it comes from, the imaging process would be impossible, since without spatial information is not possible to create an image. However, Two-photon imaging appears as a technique that allows to reconstruct images when spatial information of light is absent.

Two-photon imaging started to draw attention after Pittman's first realisation [1]. Figure 1.2 depict a schematic of the technique. A light source is divided into two paths. In one path the light is detected by a point like detector  $D_A$  that is scanned in the transverse plane. In the other path a lens and an object are followed by a detector  $D_B$  that erases the spatial information of the light. The two-photon image is retrieved by correlating the outputs of the detectors  $D_A$  and  $D_B$ .

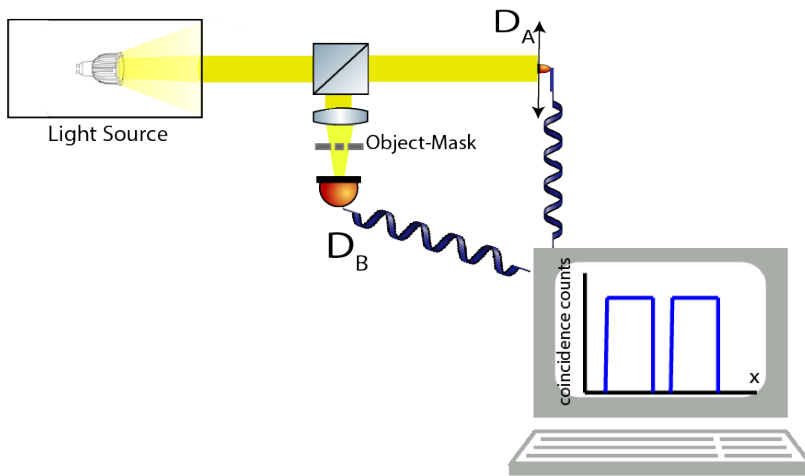


FIGURE 1.2: Two-photon imaging technique setup

There are different types of Two-photon imaging, and they differ from each other in the nature of the light source used. The first two-photon imaging realisation, done by Pittman in 1995[1], used entangled photon pairs as the light source. The second kind uses chaotic light. This light can be understood as the radiation coming from a blackbody at thermal equilibrium. Valencia *et al.* where the first ones to present an experimental demonstration of two-photon ghost imaging with thermal-like sources[6].

It is possible to reconstruct the image in this two experiments because there is some kind of correlation between the momentum of photons that are generated from the source. For the experiment with the quantum light source, the photons from a pair have negative momentum correlation. In the experiment of the chaotic light, the pair of photons present a positive correlation[7].

Historically to study the effect of Two-photon imaging with different light sources was motivated by the question about the role of entanglement in the

generation of the image. However, the role of different types of momentum correlations was not considered at that time. Recently Zhong *et al.* presented a theoretical study of the effect of different types of momentum correlations on Two-photon imaging[8]. In this monograph, we present an experiment in which it is possible to observe the effects of different types of momentum correlations on the generations of Two-photon imaging. We report preliminary results that pave the way for a more complete study that will be *pursue* by the Quantum Optics group.

In our experiment, we have done a Two-photon imaging in what is called a "lens-less two-photon image" configuration[9]. We use a source of entangled photons to which it is possible to tune the transverse momentums correlations. The pair of photons are created by using the nonlinear optical process of spontaneous parametric down conversion (SPDC) in which a laser beam is focused into a nonlinear crystal, and occasionally pairs of photons are produced. Interestingly, the geometry we used for the SPDC configuration allows us to tune the momentum correlations by adjusting the waist of pump beam[2].

This document is organized as follows: Chapter 2 presents a theoretical discussion about the fundamental aspects of the two-photon imaging, and the control of spatial correlations when using a SPDC source. In chapter 3 there is a meticulous explanation of the experimental setup used in this monograph, and its different steps. The experimental results are presented in chapter 4 and finally, conclusions and perspectives are discussed on chapter 5.

# Chapter 2

## Theory

In here, we will discuss some important facts to get a complete understanding of the physical phenomena of correlations and Two-photon imaging. Specifically, we will develop the notions that are crucial in the understanding of the Two-photon imaging using entangled light. We will start describing the process of SPDC, that provides us with the light source . Then we'll review the phenomena of imaging, looking at the standard version and the Two-photon version.

### 2.1 Correlations between two photons

The term "correlation" is crucial at this point, and it refers to the relation that two or more situations have. For example we can establish a correlations between the US dollar currency exchange rate and the prices of technology in one country. These two things have direct relation, if one blows up, the other one will too. These two situations, or variables, can have a strong correlations or a weak one.

Indeed in quantum physics we can have a pair of photons that are so strongly and specially correlated, in their possible degrees of freedom (spatial, temporal and polarization), that we say they are entangled. This statement can lead us to a dense discussion about the nature of this entanglement, a discussion that were started between Einstein and Bohr in the first years of quantum physics [10].

For the topic of this monograph it is relevant to have a pair of spatially correlated photons. This can be conveniently produced by the process of SPDC. This produces photons that are indeed entangled. However, we are not interested in this feature, Since in order to observe two photon imaging only the spatial correlations are needed.

### 2.1.1 Spontaneous Parametric Down Conversion

As the title of this work implies, we need a light source that produces pair of photons, and we would like to exploit the advantages of strong correlations between them. The photons generated via spontaneous parametric down conversion (SPDC) are widely used in quantum optics experiments. The popularity of this source of paired photons is strongly related to the relative simplicity of its experimental realisation, and to the variety of quantum features that down converted photons can exhibit. The generated photons via SPDC can be correlated in different degrees of freedom, for example in polarisation, in frequency, in orbital angular momentum and in transverse momentum [11].

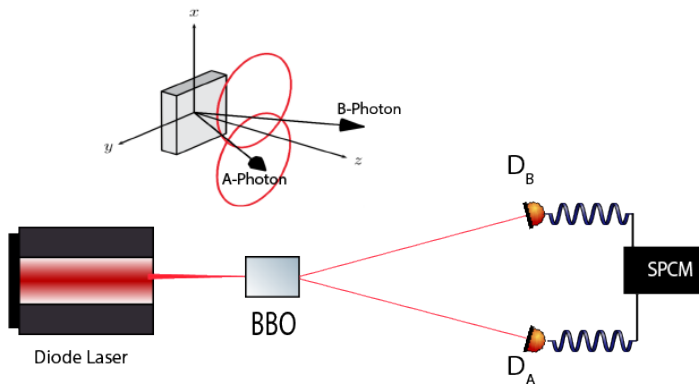


FIGURE 2.1: Simple Experimental setup for the type-II non-collinear SPDC process

SPDC is an optical process in which a pump beam propagating in the  $z$ -direction is focused into a nonlinear crystal of length  $L$ . Depending on the polarisation direction of the produced photons, the nonlinear crystals can be classified in types. The type-0 crystal will produce pairs that are polarised in the source light direction. The type-I will produce pairs that are polarised in the perpendicular direction of the pump. The last type, type-II crystals will produce a pair of photons, one with the polarisation in the same direction as the pump, and the other one in the perpendicular direction. This process can also be classified according to the geometry, the relative direction from the crystal, in which the pair of down converted photons are going to be generated. The generated pair can emerge from the crystal in a collinear or non-collinear configuration. In Figure 2.1 the non-collinear configuration is

shown, where light is generated in two separated cones, for each polarisation, these light cones intercepts in two places, from where we will use pair the pair A-photon and B-photon.

For the rest of this monography we will be focused in the type-II and non-collinear configuration. Using first order perturbation theory and the paraxial approximation, the two-photon state coming out from the crystal,  $|\Psi\rangle$ , is given by [2]:

$$|\Psi\rangle = \int d\vec{q}_B d\vec{q}_A d\Omega_B d\Omega_A \times [\Phi(\vec{q}_B, \Omega_B; \vec{q}_A, \Omega_A) \hat{a}^\dagger(\Omega_B, \vec{q}_B) \hat{a}^\dagger(\Omega_A, \vec{q}_A) + \Phi(\vec{q}_A, \Omega_A; \vec{q}_B, \Omega_B) \hat{a}^\dagger(\Omega_B, \vec{q}_B) \hat{a}^\dagger(\Omega_A, \vec{q}_A)] |0\rangle. \quad (2.1)$$

Where this state function depends on the transverse wave vectors  $\vec{q}_n = (q_n^x, q_n^y)$  and frequency detuning,  $\Omega_n = \omega_n - \omega_0^n$ , around the central frequencies,  $\omega_0^n$ , for the photon at the path  $A$  or  $B$  ( $n = A, B$ ). The  $\Phi(\vec{q}_B, \Omega_B; \vec{q}_A, \Omega_A)$  and  $\Phi(\vec{q}_A, \Omega_A; \vec{q}_B, \Omega_B)$  are the mode functions or biphotons that contains all the information about the correlations between the pair of down-converted photons. The operator  $\hat{a}^\dagger$  indicates the creations of an  $n$ -polarized photon with transverse momentum  $\vec{q}_n$ , and frequency detuning  $\Omega_n$ .

For the light source that we will use in this monograph it is enough just one of the biphotons of the Eq. 2.1. As it will shown later this later this corresponds to put a pair of polarisers before the detection of the light. The Two-photon state reduces to:

$$|\Psi\rangle = \int d\vec{q}_B d\vec{q}_A d\Omega_B d\Omega_A \times [\Phi(\vec{q}_B, \Omega_B; \vec{q}_A, \Omega_A) \hat{a}^\dagger(\Omega_B, \vec{q}_B) \hat{a}^\dagger(\Omega_A, \vec{q}_A)] |0\rangle. \quad (2.2)$$

The mode function  $\Phi(\vec{q}_B, \Omega_B; \vec{q}_A, \Omega_A)$  is related with the joint probability of detecting both an  $B$ -polarized photon, with tranverse momentum  $\vec{q}_B$  and frequency detuning  $\Omega_B$ , at the detector  $B$  and an  $A$ -polarized photon, with tranverse momentum  $\vec{q}_A$  and frequency detuning  $\Omega_A$ , at the detector  $A$ .

### 2.1.1.1 Phase matching conditions

In particular,  $\Phi(\vec{q}_B, \Omega_B; \vec{q}_A, \Omega_A)$  reads [2]:

$$\Phi(\vec{q}_B, \Omega_B; \vec{q}_A, \Omega_A) = \mathcal{N} \alpha(\Delta_0, \Delta_1) \beta(\Omega_B, \Omega_A) \times \text{sinc}\left(\frac{\Delta_k L}{2}\right) e^{i\frac{\Delta_k L}{2}}. \quad (2.3)$$

Where  $\mathcal{N}$  is a normalisation constant,  $\alpha(\Delta_0, \Delta_1)$  and  $\beta(\Omega_B, \Omega_A)$  yields the informations of the pump's transverse and spectral distribution, respectively,  $L$

is the length of the nonlinear crystal. For the process that is happening inside the crystal, there are some conditions that have to be fulfilled. These conditions are related with the energy and momentum conservations inside the parametric down conversion process. The terms  $\Delta_0$ ,  $\Delta_1$  and  $\Delta_k$  are functions that result from the phase matching conditions and read:

$$\Delta_0 = q_B^x + q_A^x. \quad (2.4)$$

$$\Delta_1 = q_A^y \cos\phi_A + q_B^y \cos\phi_B - N_B \Omega_B \sin\phi_B + N_A \Omega_A \sin\phi_A - \rho_B q_B^x \sin\phi_B. \quad (2.5)$$

$$\begin{aligned} \Delta_k = & N_p (\Omega_B + \Omega_A) - N_B \Omega_B \cos\phi_B - N_A \Omega_A \cos\phi_A \\ & - q_B^y \sin\Omega_B + q_A^y \sin\Omega_A + \rho_p \Delta_0 - \rho_B q_B^x \cos\phi_B. \end{aligned} \quad (2.6)$$

The angles  $\phi_B$  and  $\phi_A$  are the creation angles of the down-converted photons with respect to the pump's propagation direction, whereas  $\rho_p$  and  $\rho_B$  are angles, they account for the walk-off of the pump  $p$  and the  $B$  down-converted photon, respectively.  $N_n = \frac{\delta k}{\delta \omega}$  denotes the inverse of the group velocity for each photon, the inverse of the change of the angular frequency  $\omega$  against the angular wavenumber  $k$ .

### 2.1.2 Spatial Correlations

In order to observe the correlations presented in 2.3 we have to take into account some considerations about the description of the things we have in optical table. First of all we have a pump beam with a Gaussian profile with waist  $w_p$  in such way that  $\alpha(\Delta_0, \Delta_1) \propto \exp[-w_p^2(\Delta_0^2 + \Delta_1^2)/4]$ , a CW pump laser, mathematically represented by  $\beta(\Omega_B, \Omega_A) \propto \delta(\Omega_B + \Omega_A)$ . Making the approximations for the sinc function by a Gaussian function with the same width at  $1/e^2$  of its maximum, i.e.,  $\text{sinc}(x) \approx \exp(-\gamma x^2)$  with  $\gamma$  equal 0.193. The mode function reduces to:

$$\begin{aligned} \Phi(\vec{q}_B, \Omega_B; \vec{q}_A, \Omega_A) = & \mathcal{N} \beta(\Omega_B, \Omega_A) \times \\ & \exp \left[ -\frac{w_p^2(\Delta_0^2 + \Delta_1^2)}{4} - \gamma \left( \frac{\Delta_k L}{2} \right)^2 + i \frac{\Delta_k L}{2} \right]. \end{aligned} \quad (2.7)$$

As said before, we are interested in the spatial correlation that the photons exhibit. For these reason the frequency information has to be traced out. This is achieved by placing some interferometer filters before detection. This spectral filters are modeled as  $f_n(\Omega_n) = \exp[-\Omega_n^2/(4\sigma_n^2)]$ , with bandwidth

$\sigma_n$  chosen to achieve a regimen where the spatial-spectral correlations are completely broken [12]. To achieve this mathematically we have to integrate 2.7 around the time variables:

$$\tilde{\Phi}(\vec{q}_B, \vec{q}_A) = \int d\Omega_B d\Omega_A f_B(\Omega_B) f_A(\Omega_A) \Phi(\vec{q}_B, \Omega_B; \vec{q}_A, \Omega_A). \quad (2.8)$$

The Biphoton then takes a quadratic form[2]:

$$\tilde{\Phi}(\vec{q}_B, \vec{q}_A) = N \exp \left[ -\frac{1}{2} x^T A x + i b^T x \right]. \quad (2.9)$$

where N is a normalization constant, that satisfies  $\int \int |\tilde{\Phi}(\vec{q}_B, \vec{q}_A)|^2 d^2 \vec{q}_B d^2 \vec{q}_A = 1$ .  $x$  is a 4-dimensional vector defined as  $x = (q_B^x, q_B^y, q_A^x, q_A^y)$ ,  $A$  is a  $4 \times 4$  real-valued, symmetric, positive definite matrix and  $b$  is a 4-dimensional vector.  $A$  and  $b$  are defined from the phase-matching conditions of the SPDC process.  $x^T$  and  $b^T$  denote the transpose of  $x$  and  $b$ .  $A$  and  $b$  are functions that depend of all the relevant parameters in the experiment such as the length of the crystal L, pump waist  $w_p$ , creation angles inside the crystal  $\varphi_n$  and the width of the spectral filter  $\sigma_n$ .

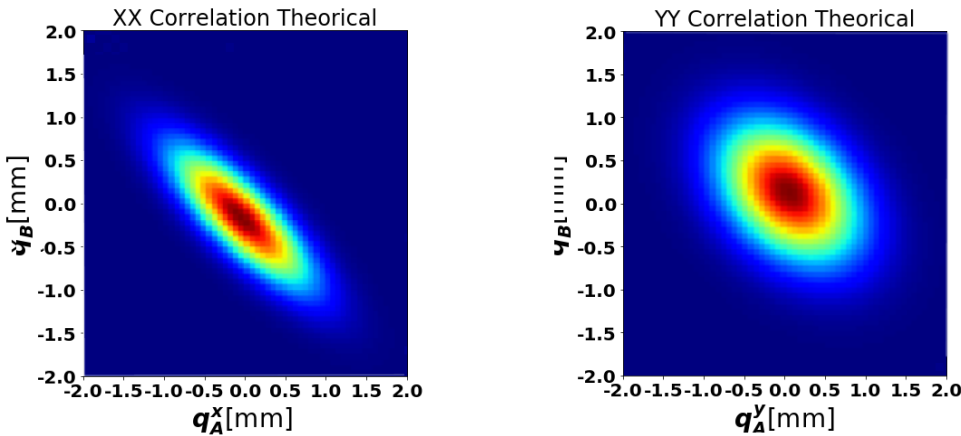


FIGURE 2.2: Theoretical Spatial correlations between a pair of down-converted photons,  $w_p = 91\mu m$

Figure 2.2 show a pair of examples of how these correlations we are talking about look like. These correlations have elliptical shape, and show how strong is the possibility of detecting a photon at a given momentum. For example, looking at XX Correlation, there is a great chance of detecting simultaneously a photon at  $q_B^x = 0$  and at  $q_A^x = 0$ . Now if we keep looking at this XX correlation, we can also observe that detecting a photon at  $q_B^x = 0.5$ , would constrain the possible values of  $q_A^x$  to values close to  $-0.5$ . This change in the sign is an evidence of an anticorrelation between the photons in the XX

direction. In Figure 2.2 we can also find the theoretical YY correlation. For this case we have a less narrower elipsis, meaning we have a less strong correlation in the YY direction. If we detect a photon at  $q_B^y = 0.5$ , we would probably get another photon in the path A between  $[-0.5, 0.5]$  with almost equal probability for this range. It is clear that the more this correlations look like a circle, the correlation is less stronger . In contrast between more narrower the elipsis is, the stronger the correlation is. Another important fact from this analisys is that the direction of the elipsis give us a sense of the sign of the correlation, a negative correlation is called an anticorrelation.

It is easy to think how a strong correlation should look like, a strong correlations in spatial variables would mean that if we have the position of one photon at the position  $\vec{q}_B$  we immediately would know which  $\vec{q}_A$  have the other photon, this kind of ideal spatial correlation would look like a straigth line really thin. Figure 2.3 shows this ideal correlation that would be like having a relation of  $\delta(\vec{q}_b - \vec{q}_a)$ .

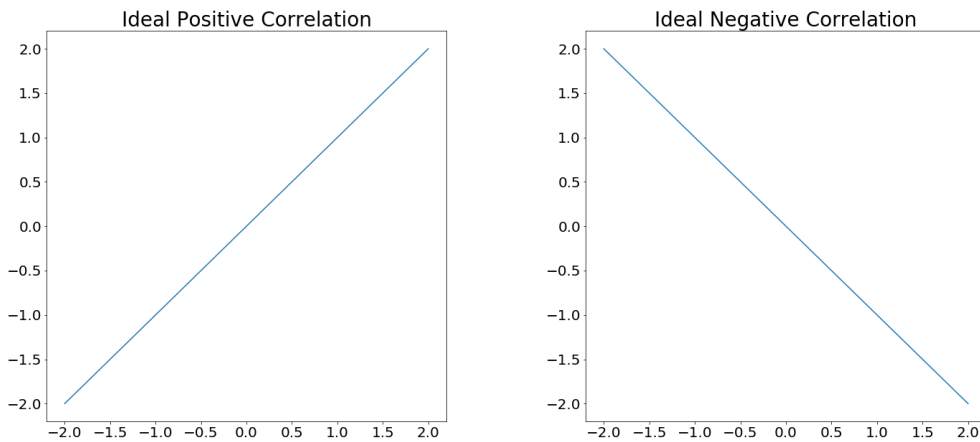


FIGURE 2.3: Positive and Negative ideal spatial correlations

In the frame of this discussion, it would be useful to define a way to quantify the degree of spatial correlation. We shall define a 'correlation parameter':

$$K^\lambda = \frac{C_{si}^\lambda}{\sqrt{C_{ss}^\lambda C_{ii}^\lambda}}, \quad (2.10)$$

calculated for each direction ( $\lambda = x, y$ ) from the covariance matrix  $C^\lambda$  with elements  $C_{kj}^\lambda = \langle q_k^\lambda q_j^\lambda \rangle - \langle q_k^\lambda \rangle \langle q_j^\lambda \rangle$ . This 'correlations parameter' is a measure of the linear correlation between two variables, in this case  $q_A^\lambda$  and  $q_B^\lambda$ .

### 2.1.3 Tunable Spatial Correlation SPDC source light

It is clear that both 2.7 and 2.8 depend on  $w_p$ , the pump waist. If we change this parameter and keep the rest of the parameters constant, the term in the exponential function  $[-w_p^2(\Delta_0^2 + \Delta_1^2)/4]$  will variate, making changes in the shape of the original mode function. As it was mentioned here before and in [2], the mode function contains all the informations about the correlations of the generated down converted photons. Hence changing the pump waist  $w_p$  will change the correlations of the generated pair of photons. In Figure 2.4 is shown a new pair of correlations, but this ones correspond to a different pump waist  $w_p$ . We can see the differences with the ones presented in Fig. 2.2, in this case we have a positive correlation in the YY direction, meaning that we won't have a change of sign for  $q_y^y$ . Also, for this case, we have a stronger correlation in the YY direction and we still have a anticorrelation in the XX direction, but this time is a weaker correlation.

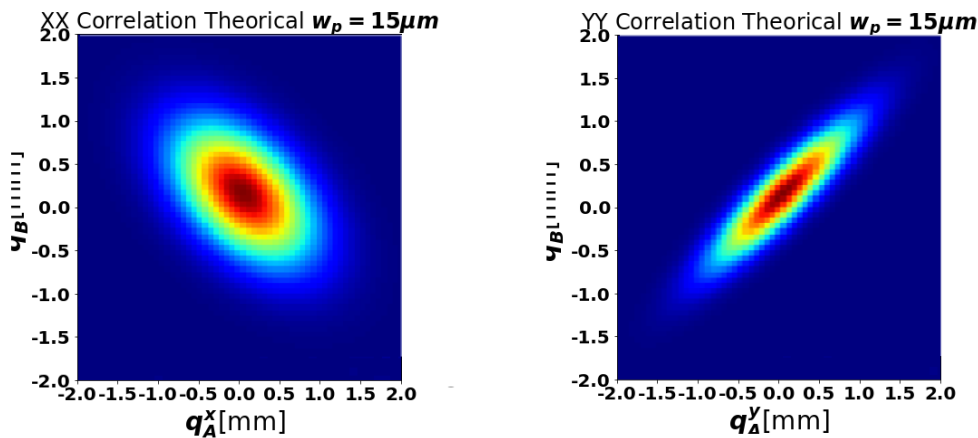


FIGURE 2.4: Simulated correlations  $w_p = 15\mu m$

## 2.2 Imaging

As said in the introduction, imaging is a process in which we make a reconstruction of an object using the spatial information of the light that were reflected, or scattered from that object. This representation of the object can not be an exact copy. For example, when we forget our glasses, we see our surroundings blurred. The difference between having or not our glasses is that they will boost up our spatial resolution of the objects.

## 2.2.1 Standar Imaging

The concept of optical imaging was well developed in classical optics and the Figure 2.5 schematically illustrates a standar imaging setup. In this setup an object is illuminated, an imaging lens is used to focus the scattered and reflected light from the object onto an image plane which is defined by the "Gaussian thin lens equation"[5]:

$$\frac{1}{S_o} + \frac{1}{S_i} = \frac{1}{f}, \quad (2.11)$$

where  $S_o$  is the distance between the object and the imaging lens,  $S_i$  the distance between the imaging lens and the image plane, and  $f$  the focal length of the imaging lens. This equation defines a point-to-point relationship between the object plane and the image plane: any radiation starting from a point on the object will collapse at a certain point at the image plane.

This one-to-one correspondence in the image-forming relationship between

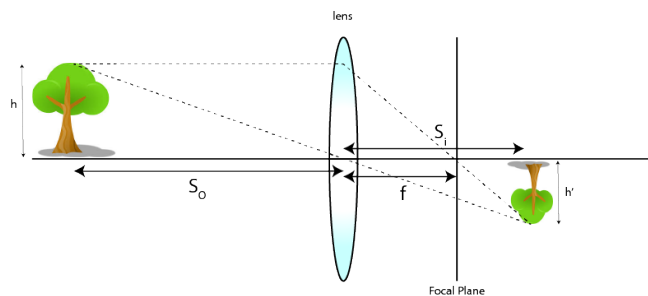


FIGURE 2.5: Optical imaging: a lens produces an image on an object at  $S_i$ . This distance is defined by the Gaussian thin-lens equation

the object and the image planes produces a perfect image. The observed image can be magnified or demagnified, for example, in the Figure 2.5 the original object is a tree, and it is demagnified at the image plane. This depends on which optical system are we using, what kind of lenses are involved and the distance between object and lenses.

The observed image is a reproduction of the illuminated object, mathematically corresponding to a convolution between the object distribution function  $|T(\vec{r}_o)|^2$  (aperture function) and a  $\delta$ -function, which is present for the perfect point-to-point correspondence [13]:

$$\langle I(\vec{r}_i) \rangle = \int_{obj} d\vec{r}_o |T(\vec{r}_o)|^2 \delta(\vec{r}_o + \frac{\vec{r}_i}{m}), \quad (2.12)$$

where  $\langle I(\vec{r}_i) \rangle$  is the mean intensity at the image plane,  $\vec{r}_o$  and  $\vec{r}_i$  are 2-D vectors of the transverse coordinates,  $\vec{r}_n = (x_n, y_n)$ , in the object and image planes, respectively, and  $m = S_i/S_o$  is the image magnification factor.

In a more real situation, we are limited by the finite size of the optical system, we may never obtain a perfect image. The oscillating photons that form the image have constructive-destructive interference, turning the point-to-point correspondence into a point-to-"spot" relationship. The  $\delta$ -function in the convolution of equation 2.12 will be replaced by a point-to-"spot" image-forming function, or a point-spread function,

$$\langle I(\vec{r}_i) \rangle = \int_{obj} d\vec{r}_o |T(\vec{r}_o)|^2 \text{somb}^2 \left[ \frac{\pi D}{\lambda S_o} \left| \vec{r}_o + \frac{\vec{r}_i}{m} \right| \right], \quad (2.13)$$

where the sombrero-like point-spread function is defined as  $\text{somb}(x) \equiv 2J_1(x)/x$ , with  $J_1(x)$  the first-order Bessel function,  $D$  the diameter of the imaging lens and  $\lambda$  the wavelength of the light used. the finite size of the spot is defined by  $J_1(x)$  and determined by the ratio  $D/\lambda S_o$ . In Figure 2.6 we can appreciate the behaviour of the sombrero-like function for different constants. The constants are define as  $C = \frac{\pi D}{\lambda S_o}$  where we have to note some things in order to understand this function. First of all  $\lambda$  is the light that we are using for the imaging process, so in the frame of this discussion about standar imaging, the light that is going to be used, is the light that the human eye can see ( $\sim 390 - 700\text{nm}$ ). Restricting the light that is going to be used leave us with two parameters to change. If we asume we will stay at a fixed distance  $S_o$ , Figure 2.6 shows us that a narrower point-spread function is achievable increasing the size of the lens.

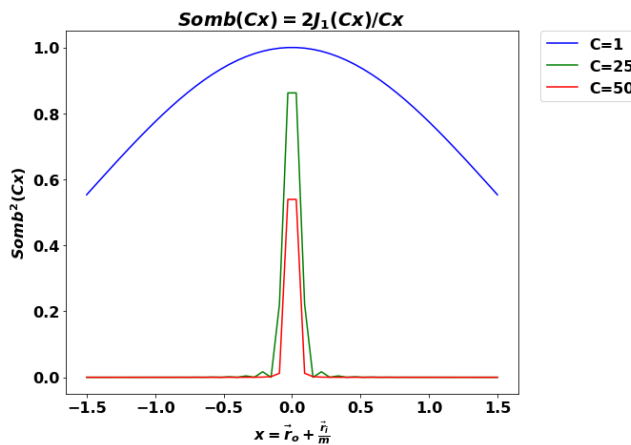


FIGURE 2.6: sombrero-like function behaviour for differents constants

A narrower point-spread function turn into a high spatial resolution. Another daily situation in which we are forming images, is when we take a picture. Cameras manufactureres play with this functions to achieve a high spatial resolution, a spot-to-pixel correspondence. For further informations about this "real life" situation check[13] chapter 4 for further development.

### 2.2.2 Two-photon Imaging

Two-photon imaging consist in reconstructing an image of an object. But in this case we use two dectector located in the two different paths of the light. In Figure 2.7 we can appreciate a simple setup of the Two-photon technique. We separate the light beam in two different paths, the photons travelling through the A path will reach a  $D_A$  point like detector, this detector have the ability to scan in the transverse direction.

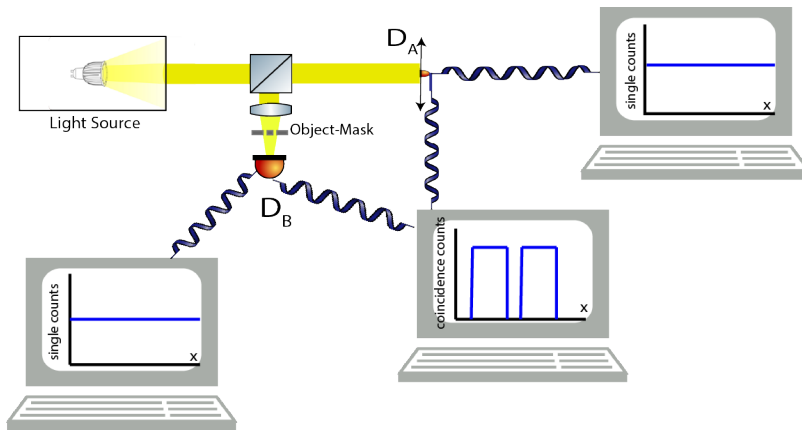


FIGURE 2.7: Simple schematic for the Two-photon Imaging.  
Only in the coincidence counts we can reconstruct the image

The light that were reflected in Figure 2.7 is denominated the B path. This light goes through a imaging lens and then interacts with an object. After this, all light is collected by a  $D_B$  bucket detector, this detector loses all the spatial information about the light. When we scan the  $D_A$  detector in the transverse direction, we get a constant single counts, with no information what so ever about the object. When counting the photons that reached  $D_B$  we also get a constant signal. However, if we go to the coincidence regime between  $D_A$  and  $D_B$ , we are able to reconstruct the image. This is done by counting every time we have a photon detected going throught the object  $D_B$ , and a photon at a certain position  $D_A(x_i)$  simultaneously.

The standar imaging used the photons at the image plane to form the image. In other words it measures one photon per spot at the image plane.

For the two-photon imaging, in certain aspects the behaviour is similar as that of the classical. They both exhibit a similar point-to-point imaging-forming function, except the two-photon image is only reproducible in the joint-detection between two independent photodetectors, and the point-to-point imaging-forming function is in the form of second-order correlation,

$$R_{BA}(\vec{r}_A) = \int_{obj} d\vec{r}_B |T(\vec{r}_B)|^2 G^{(2)}(\vec{r}_B, \vec{r}_A), \quad (2.14)$$

where  $R_{BA}(\vec{r}_B)$  is the joint-detection counting rate between photodetectors  $D_B$  and  $D_A$ .  $G^{(2)}(\vec{r}_B, \vec{r}_A)$  is a second-order correlation function, corresponding to the probability of observing a joint photo-detection event at the coordinates  $\vec{r}_B$  and  $\vec{r}_A$ . The physics behing  $G^{(2)}(\vec{r}_B, \vec{r}_A)$  is what changes between the light source used.

This second-order correlation functions is defined as[13]:

$$G^{(2)}(\vec{r}_B, \vec{r}_A) = \frac{\langle E^*(\vec{r}_B)E^*(\vec{r}_A)E(\vec{r}_B)E(\vec{r}_A) \rangle}{\langle |E(\vec{r}_B)|^2 \rangle \langle |E(\vec{r}_A)|^2 \rangle}. \quad (2.15)$$

Where  $E(\vec{r}_n)$  and  $E^*(\vec{r}_n)$  are the electrical field and complex conjugate at the point  $r_n$  with  $n = A, B$ .  $E(\vec{r}_n)^2$  is defined by  $E^*(\vec{r}_n)E(\vec{r}_n)$ , and  $\langle \dots \rangle$  stands for a statistical average.

### 2.2.2.1 Lensless Two-photon Imaging using entangled photon

In the previous section we introduced the notion of two-photon imaging , but we didn't care much about the nature of the light source. For this monograph we will use entangled photon as the light source. For now on we will focus on decribing the experimental setup presented in Figure 2.8. A diode laser is used to pump a BBO crystal, as a result of the SPDC process, we obtain a pair of entangled photons in a noncollinear configuration. The down converted pairs travels through a 2-f system. The A photon is then detected by  $D_A$ . In the path of the B photon, we place the object and then it is the  $D_B$  bucket detector. It is important to note that in this setup there is no imaging lens, the used lenses are to define a very special plane at 2f distance from the crystal, we will discuss about it later in this section.

The main point of the section is to calculate Eq 2.14 for this situation, we need to know the state of the biphoton at the output of the crystal,  $\tilde{\Phi}_c(\vec{q}_c, \vec{q}_c)$

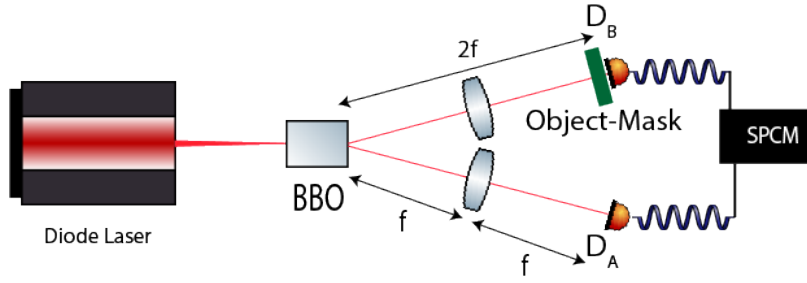


FIGURE 2.8: Simple schematic for a Two-photon Imaging using entangled photons and a 2-f system

Then from this result we can use the fresnel propagation theory to analytically model the biphoton propagation in any arbitrary Two-photon Imaging/Lensless Two-photon Imaging setup. This propagation is done by determining the Green function of the optical path by which the beams will travel[14].

Since both path A and B have an identical 2-f system, we are at the called Fourier plane. It is well known that when the light goes through this system suffers a Fourier transform[13]. It means that there is a relation between the initial  $q_c$  initial transverse momentum at the crystal, and the  $r_f$  final position of the photons. This relation is:

$$\vec{q}_{initial} = \frac{2\pi}{\lambda f} \vec{r}_{final}, \quad (2.16)$$

where  $\vec{q}_{initial}$  is the transverse momentum of the light before the 2-f system,  $\vec{r}_{final}$  is the position of photon after going through the lens and traveling a 2-f distance.  $f$  stands for the focal length of the lenses used and  $\lambda$  wavelength.

The Green function that propagates light with transverse momentum  $\vec{q}$  from the source, to the Fourier plane located at a position  $\vec{r}_f$  is[14]:

$$G(\vec{q}, \vec{r}_f) = \int d^2\vec{r}_l \int d^2\vec{r}_c h(\vec{r}_f - \vec{r}_l, f) L_f(\vec{r}_l) h(\vec{r}_l - \vec{r}_c, f) e^{i\vec{q} \cdot \vec{r}_c}. \quad (2.17)$$

With  $\vec{r}_c$  and  $\vec{r}_l$  denoting the transverse position vectors in the plane of the crystal and the lens respectively.  $h(\vec{r}_f - \vec{r}_l, f)$  and  $h(\vec{r}_l - \vec{r}_c, f)$  are the Fresnel propagators<sup>1</sup> that propagates light from  $\vec{r}_l$  to  $\vec{r}_f$  and  $L_f(\vec{r}) = \Psi(\vec{r}, -f)$  is the thin-lens transfer function associated to a lens[14].

Taking advantage of the 2-f system as a Fourier transform to reduce the

<sup>1</sup>Fresnel Propagator:  $h(\vec{r}, z) = (-\frac{i}{\lambda z}) e^{(i\frac{2\pi z}{\lambda})} \Psi(\vec{r}, z)$  with  $\Psi(\vec{r}, z) = e^{(i\frac{\pi}{\lambda z})\vec{r}^2}$ .

amount of calculations , using the relation 2.16, and after solving the integrals over  $r_l$  and  $r_c$ , equation 2.17 can be written as:

$$G(\vec{q}, \vec{r}_f) = Ce^{\frac{i\pi}{\lambda f} \vec{r}_f^2} e^{\frac{i\lambda f}{4\pi} \vec{q}^2} \delta(\vec{q} - \frac{2\pi}{\lambda f} \vec{r}_f), \quad (2.18)$$

where C is a complex constant. Then we can finally propagate the biphoton function in terms of transverse momenta. Where  $\Phi_1(\vec{q}_B, \vec{q}_A)$  is the biphoton after traveling through two arbitrary optical paths, it can be expressed in terms of the corresponding Green functions and the initial biphoton function,  $\tilde{\Phi}_c(\vec{q}_c, \vec{q}_c)$ , as:

$$\Phi_1(\vec{q}_B, \vec{q}_A) = G_B(\vec{q}_B, \vec{r}_B) G_A(\vec{q}_A, \vec{r}_A) \tilde{\Phi}_c(\vec{q}_c, \vec{q}_c), \quad (2.19)$$

where  $\vec{r}_B$  and  $\vec{r}_A$  denotes the photon position in the transverse plane at a 2-f distance from the crystal, the subscript stand for the different path followed by light, Figure 2.8. The  $G_B(\vec{q}_B, \vec{r}_B)$  and  $G_A(\vec{q}_A, \vec{r}_A)$  are the green functions for each path, defined as in equation 2.18, they are:

$$G_B(\vec{q}_B, \vec{r}_B) = G(\vec{q}_B, \vec{r}_B) \times T(\vec{r}_B). \quad (2.20)$$

$$G_A(\vec{q}_A, \vec{r}_A) = G(\vec{q}_A, \vec{r}_A). \quad (2.21)$$

Where  $T(\vec{r}_B)$  is the transfer function of the object, which is only present at the B path, Figure 2.8. Gathering all the previous results we can obtain  $\Phi_1(\vec{r}_B, \vec{r}_A)$ . This is done by replacing Eq. 2.20 and 2.21 into Eq. 2.19, then evaluating the integrals over the transverse momentum, we obtain:

$$\Phi_1(\vec{r}_B, \vec{r}_A) = C^2 T(\vec{r}_B) \Phi(\frac{2\pi}{\lambda f} \vec{r}_B, \frac{2\pi}{\lambda f} \vec{r}_A). \quad (2.22)$$

This function describes the biphoton at the planes of the object and the scanning detector. It shows that the biphoton at the 2-f plane as a function of  $\vec{r}_B$  and  $\vec{r}_A$ . If we take a closer look, this result enable us to compute the biphoton at the 2-f plane by using Eq 2.9 without the need to actually calculate its propagation, just by evaluating it with the Fourier relationship, 2.16. This is specially usefull when we try to simulate this on a computer, the amount of calculations is significantly reduced by this fact.

As described at the beginning of this Section 2.2.2, we lose all the spatial information about the photon that interacts with the Object, B path, and this is done by placing a bucket detector that gathers all light and send it to a multimode optic fiber, without saving any information about the position of

the photons in this path. From the mathematical point of view, the bucket detector is modeled as:  $\Phi_1(\vec{r}_A) = C^2 \int d^2\vec{r}_B T(\vec{r}_B) \Phi(\frac{2\pi}{\lambda_f} \vec{r}_B, \frac{2\pi}{\lambda_f} \vec{r}_A)$ . Using the fact that the coincidence counts that will be measured by the Detectors will be proportional to the magnitude square of the resulting biphoton function  $\Phi_1(\vec{r}_A)$ [13].

$$R(\vec{r}_A) \propto |\int d^2\vec{r}_B T(\vec{r}_B) \Phi(\frac{2\pi}{\lambda_f} \vec{r}_B, \frac{2\pi}{\lambda_f} \vec{r}_A)|^2 \quad (2.23)$$

Where  $R(\vec{r}_A)$  is the function that describes de coincidences counts between de detectors  $D_B$  and  $D_A$  in Figure 2.8.  $R(\vec{r}_A)$  is a function of the spatial positions,  $(x_A, y_A)$  of the detection plane at  $D_A$ . This function  $R(\vec{r}_A)$  have the expected behaviour described by  $R_{BA}(\vec{r}_A)$  in Eq. 2.14, where the second-order correlation function in this case is  $\Phi(\frac{2\pi}{\lambda_f} \vec{r}_B, \frac{2\pi}{\lambda_f} \vec{r}_A)$ , as we said, the function containing all the informations about the correlations between the pair of down-converted photons. Moreover, Equation 2.23 indicates that the form of  $\Phi(\vec{q}_B, \vec{q}_A)$  determines if  $T(\vec{r}_B)$  can be recovered in the coincidence count. Additionally, the type of spatial correlation in  $\Phi(\vec{q}_B, \vec{q}_A)$  defines the orientation of the image obtained.

### 2.2.2.2 Effect of the different spatial correlations

If we want to observe the effect of differents spatial correlations in the obtained image, we need to take a look at Eq. 2.23. This equation describes me the obtained image as a function of the Biphoton. In here is where the spatial correlations are indicated, changing the spatial correlations would mean to change the  $\Phi(\frac{2\pi}{\lambda_f} \vec{r}_B, \frac{2\pi}{\lambda_f} \vec{r}_A)$ . As said before, this experiment is a big project of the Quantum Optics group that was running way before this monograph was started. This Eq 2.23 can be numerically solved, and this was done by one former group member. We can obtain numerically the behaviour of  $|\Phi(\frac{2\pi}{\lambda_f} \vec{r}_B, \frac{2\pi}{\lambda_f} \vec{r}_A)|^2$ . In Figure 2.9 there are two Two-photon images, each one of them corresponds to a different pump waist. The correlations for  $w_p = 15\mu m$  are in Figure 2.4, these correlations are related with the image we obtained. In the image for  $w_p = 15\mu m$  we observe a wider elipsis for the  $x$  values, while having a narrower part for the  $y$  values. This is related to what was mentioned before, for this waist, the YY correlations was stronger and positive, while for XX correlations we had a weaker anticorrelation. This anticorrelation is observed in the change of position in the  $x$  direction.

In the Figure 2.9 we also find the Two-photon image for  $w_p = 91\mu m$ . The correlations for this waist are in Figure 2.2, where we have a strong correlation in the XX direction and both of them are anticorrelations. The image

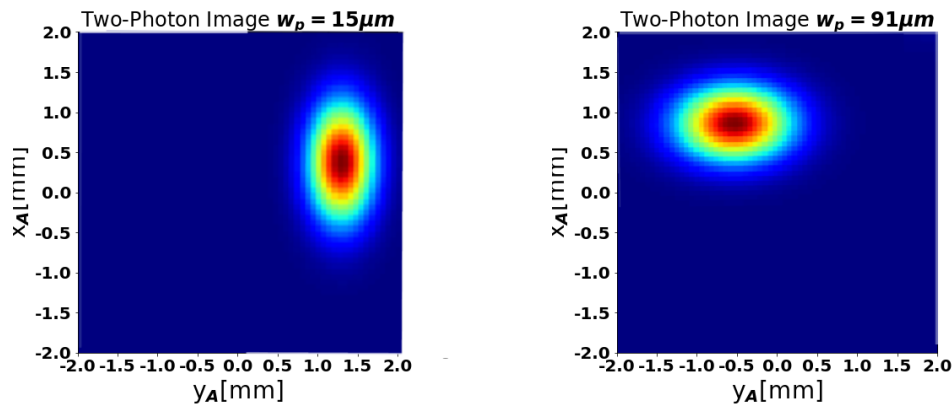


FIGURE 2.9: Simulated Two-photon images for two different waist,  $w_p = 15\mu m$  and  $w_p = 91\mu m$ , Where  $T(\vec{r}_B)$  is an square in the second quadrant.

change completely its original position in both direction, the photons present an anticorrelation. We had a weaker correlation in the YY direction, meaning loose spatial resolution in this direction.

# Chapter 3

## Experimental Setup

In the following chapter, we will look in detail the components of the experimental setup to observe the effects of different spatial correlations in a lensless quantum image experiment. The setup consist of two main stages. The first one is the light source with tunable spatial correlations, and the second one the two-photon imaging system. This experimental setup located at the optical table of the Quantum Optics Laboratory.

### 3.1 Light Source with Tunable Spatial Correlations

The experimental setup to obtain pairs of photons is shown in Figure 3.1. The source consists of a type-II crystal in non-collinear configuration. The source is based on spontaneous parametric down conversion.

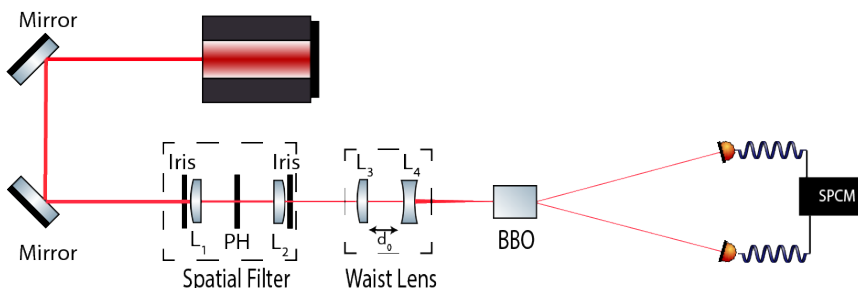


FIGURE 3.1: Experimental Setup for the SPDC light Source

To obtain pairs of photons by means of SPDC, we need to pump a nonlinear crystal. For this experiment, we use a diode laser (Crystal Laser model No. DL 405-200), that delivers a continuous wave(CW) at wavelength  $\lambda = 406,101\text{nm}$  and  $\Delta\lambda = 4\text{nm}$ . The laser delivers light at 200 mW with a beam diameter of 1.5 mm and a beam Divergence of 1.2 mrad.

As seen in Figure 3.1, we redirect the laser beam two times, for doing so we use a pair of mirrors. For this kind of experiments, when the efficiency of the optical elements is really important, it is important to use the correct type

of mirror, we want a mirror that reflects most of the light. For this reason, depending on the wavelength it is possible to find mirrors and lenses with different types of coating. Mirror and Lenses have a thin layer that is more efective for a range of wave lengths. For our experiment the mirrors have a coating that highly reflects light at  $405nm$ . It is possible to manipulate the direction in which the mirror will reflect the light by using an appropriate mount with screws that allows to move the reflected beam in one direction. In the experimental setup we use two mirrors to change the direction two times.

### 3.1.1 Spatial Filter to achieve a Gaussian pump beam

As seen in theory we need a gaussian beam to pump the crystal. In our experiment we have a diode laser whose spatial profile is not a Gaussian. This ramdom spatial profile is a result of the randomnes in the quantum emissions and absorptions that are happening at the exited atoms at the diode laser[5]. In order to achieve a Gaussian profile, we use the spatial filter presented in the Figure 3.1. The spatial filter is composed by two irises, an Aspheric Lens of  $f = 30mm$ (LA1805-A), a pinhole of  $50\mu m$  and a collimating lens of  $f = 60mm$ (LA1134-A).

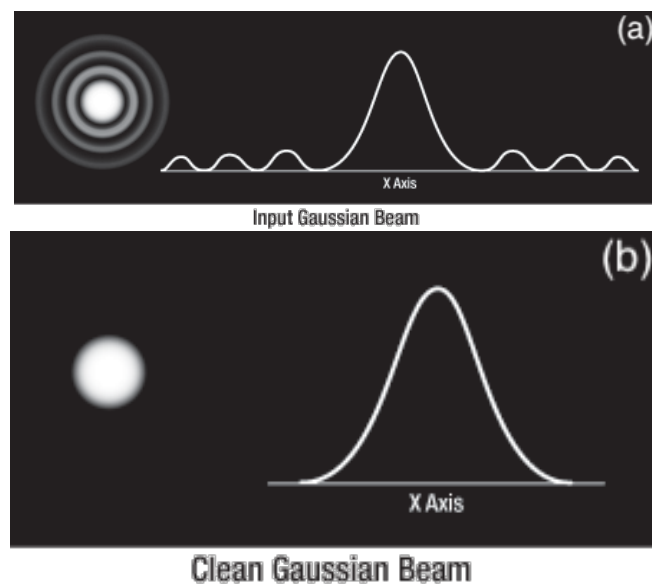


FIGURE 3.2: The spatial intensity profile before and after the spatial filtering process , Taken from [4]

To undestand what a spatial filter does consider a light beam with a spatial profile as the one depicted in Figure 3.2(a). After passing a spatial filter

the obtained light beam look like the one in Figure 3.2(b), that is now the Gaussian profile we were looking for.

In Figure 3.3 we can appreciate the spatial intensity profile of the pump beam just after it goes through the spatial filter, the red line is a fit done computationally. The green dots are the measured waist at 3 given percentages of intensity, 13.5%, 50% and 80% respectably. The tool we used to measure this is called Beam Master, and it have its own spatial directions, V and W direction . In the optical table we made sure that the V and W direction agreed with our x and y directions. The waist of a gaussian beam propagating in the z direction is given by[15]:

$$w(z) = w_0 \sqrt{1 + (z/z_R)^2}. \quad (3.1)$$

Where  $z_R$  is the *Rayleigh length* and it's defined as  $z_R = \frac{\pi n w_0^2}{\lambda_0}$ . The previous expresion is a function of  $n$  the refractive index,  $\lambda_0$  the wavelength of the beam and  $w_0 = w(0)$  the waist at the origin.

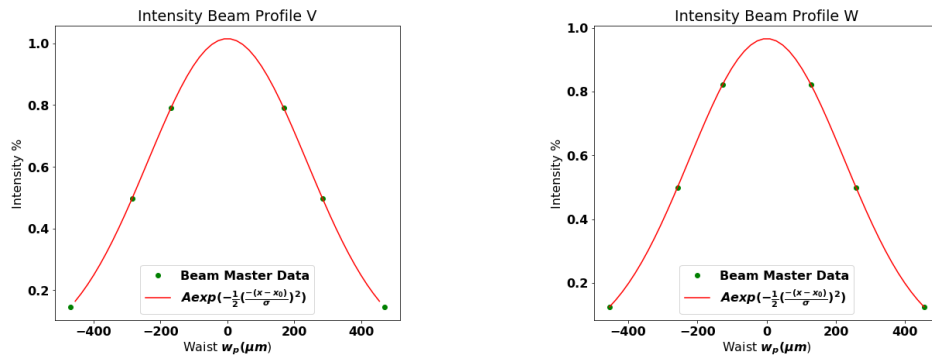


FIGURE 3.3: The spatial intensity profile measured after the spatial filter

### 3.1.2 Lenses to Control the pump beam waist

After successfully achieving a Gaussian profile, which is important for the reasons described in Section 2.1.2, we need a way to control the pump waist, but we need to do it in a way not too complicated, that doesn't imply too many changes in the experimental setup. Putting a lens, in the beam propagation direction, with certain focal lenght  $f$  will define a zone around the distance  $f$  called *Focus depth*[5], where in the middle we find the narrowest point of the beam. The radius of this zone is:

$$W_0 = \frac{\lambda f}{\pi W_B}. \quad (3.2)$$

Where  $W_B$  is the width of beam at the lens. In Figure 3.4 we see this behaviour. If we want to change  $W_0$ , we need to use a different lens with  $f'$  a different focal length. This will produce also a different *Focus depth*. Therefore, if we want to focus the beam at a fixed distance  $F$ , using this method to control the pump waist is not practical. Every different lens we would use will make this waist  $W_0$  at a different distances  $f$ . It is necessary to find a combination of lenses, that we will call *waist lens* that make us a  $W_0$  at a transverse plane located in a fixed position  $F$  from the set. In Figure 3.5 we present the combination of lenses, *waist lens*. It consists on an arrangement of two lenses, a positive and a negative one, separated a distance  $d_0$  from each other.

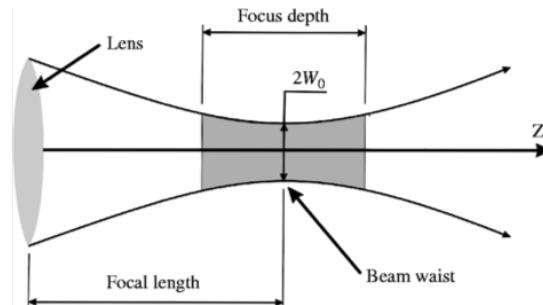


FIGURE 3.4: Effect of lens on a Gaussian beam[5]

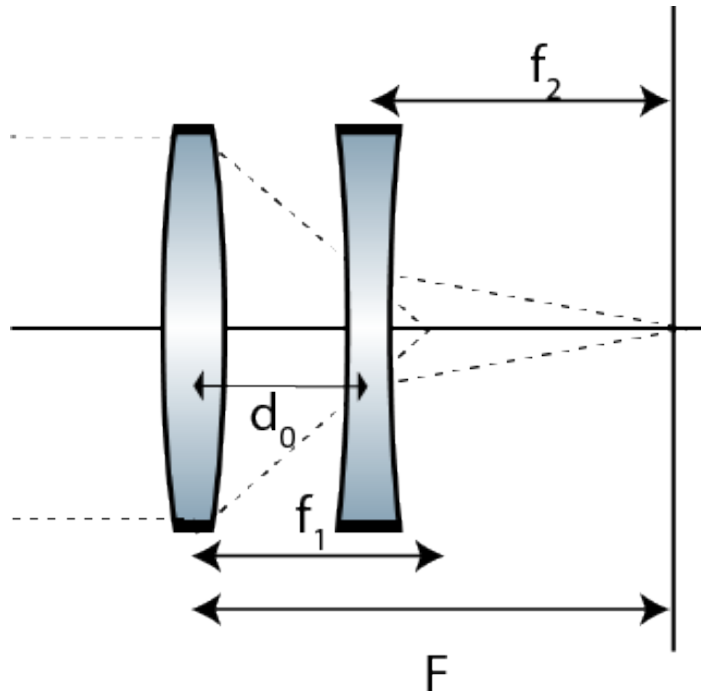


FIGURE 3.5: Composition of lenses to control the Pump Waist at a Fixed distance  $F$

We can define a *effective focal length*  $F$  as a function of  $f_1$  and  $f_2$ , the focal lengths of the positive and negative lenses respectively. With the constrain that  $d_0 < f_1$ ,  $F$  reads:

$$F = \frac{f_1 |f_2|}{|f_2| - f_1 + d_0}. \quad (3.3)$$

This new effective focal length is crucial in the realisation of this experiment, as described before, we are interested in observing the effect in the reconstructed image using different spatial correlations. This is done by changing the pump waist of the laser that is focused on the crystal. It is not experimentally practical to be changing the crystal position, it would mean to change the position of all the optical elements that follows. For this reason, it is perfect to be able to achieve the desired pump waist just by changing the relative separation of two lenses.

### 3.1.3 BBO(Beta Barium Borate) Crystal: The source of pair of photons

The Beta Barium Borate (BBO) is an inorganic compound, with chemical formula  $\beta\text{-BaB}_2\text{O}_4$ . This crystal is a nonlinear optical media commonly used. It is also a birefringent<sup>1</sup> material and its transmission regions extends from  $189\text{nm}$  to  $3500\text{nm}$ [16]. The type-II crystal is mounted in such way that the input and output plane are fixed. In particular the input plane is at  $F$  from the *waist lens* presented in the previous section, the power of the pump at this point is  $\sim 60\text{mW}$ . The generated photons doubles the wavelength of the original pump, it means the generated photon are around  $810\text{nm}$ .

At this point we have as a result of the SPDC process a pair of entangled photons, which have a strong correlation. This correlation is the feature in which we are interested on. We need to observe the shape of this correlations functions and the next section will focus on the experimental setup that will allow us to observe this.

## 3.2 Spatial Correlations Measurement Setup

From this point we will talk about a pair of correlated photons, that will come from the output plane of the BBO crystal, for historical reasons this photons are labeled as *signal* and *idler*. Nevertheless, to keep the same notations used

---

<sup>1</sup>Birefringence is a optical property of some materials of having a refractive index that depends on the polarisation and the propagation of light[5]

through this monograph, this photon are going to be labeled as A-photon and B-photon, depending on which path they follow, in Figure 3.6 we can see the experimental setup for measuring the spatial correlations.

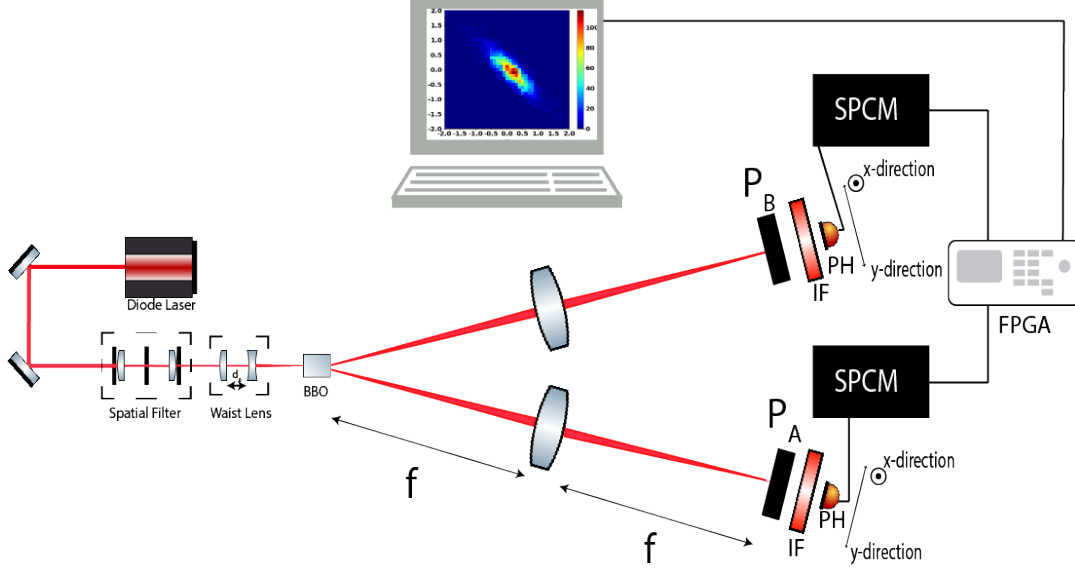


FIGURE 3.6: Experimental Setup for Obtaining the spatial correlations of a pair of down-converted photons

Observing the theory developed before there is a relation between the transverse momentum  $\vec{q}_n$  of the light before the 2-f system, and the photon position  $\vec{r}_n$  after de system, Eq. 2.16. For this reason we placed two lenses, one in each path of the light. Doing this will put our detections in the Fourier plane. We use two lenses(LA1708) of  $f = 200.0\text{mm}$  in front of each A and B. It is also important to note that from now on, the lenses and mirror used from here, will have a coating that transmits light around  $810\text{nm}$  with high efficiency for the lenses, and highly reflects light at this wavelength.

We are interested in just a pair photons,  $\Phi(\vec{q}_B, \Omega_B; \vec{q}_A, \Omega_A)$ , that are polarised in certain direction. In order to filter the others photons  $\Phi(\vec{q}_A, \Omega_A; \vec{q}_B, \Omega_B)$ , and obtain the Eq. 2.2, we place a pair of polarisers at both paths. A polariser is an optical element that filters light depending on the direction of the electrical field. We used a pair of Polarisers(WP25M-UB), which consist of an array of parallel metallic wires sandwiched between glass with certain coating for better transmission.

As pointed out in Section 2.1.2, in order to observe the transverse correlations, the frequency information has to be traced out. For doing so, we placed a pair of Interferometer Filters(IF), Thorlabs FB810-10. They are modeled as  $f_n(\Omega_n) = \exp[-\Omega_n^2/(4\sigma_n^2)]$ , where for this specific case  $\Omega_n = 810\text{nm}$  and

$\sigma_n = 2nm$ . This optical elements have the special feature that only transmits light that comes through this range of frequencies.

### 3.2.1 Detection Module

To observe the spatial correlations we have to be able to measure light that is propagating in the z-direction. Figure 3.7 shows the plane that is being scanned, where each square have a  $x_i$  and  $y_j$  position,  $i, j$  goes from 0 to  $N$ . With the help of a motorised translational stages, we can make this  $N \times N$  steps. We can control the movement of a pin hole detector, which consists in a single mode optical fiber tip. The translational stages are controlled by Arduinos, this enable us to do the scan in a complete automated way.

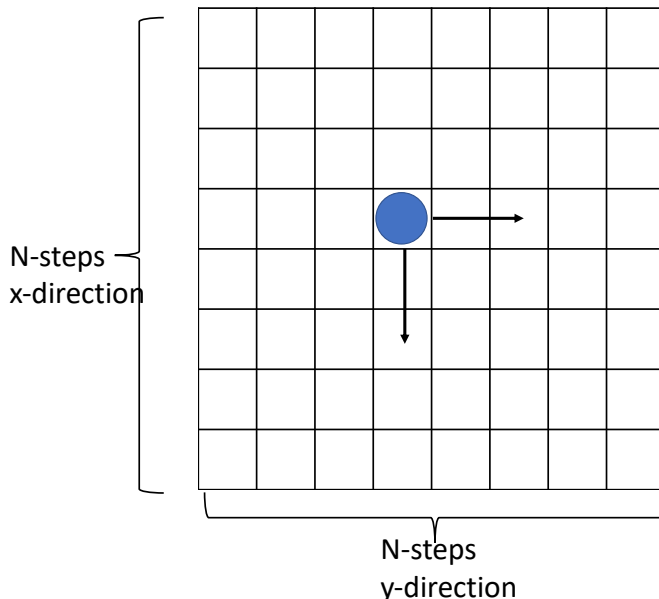


FIGURE 3.7: The plane that is being scanned by the fiber tip, it is a  $4 \times 4mm$  square, that can be scanned in  $N$  steps, where  $N$  is defined by us

Another feature that is easily controlled, is the exposure time. It means we can set how many seconds, is going to be the fiber tip at every  $(i, j)$  position. A greater time means more photon counted, and with a bigger amount of data of photons counted per position, the means values per position gives a better image, with better contrast. The places where we don't have photons tend to have a low mean value of photons counted, while the more intense places keep counting, hence having bigger means values. The  $(i_B, j_B)$  position and  $(i_A, j_A)$  position are related with  $\vec{q}_B = (q_i, q_j)$  and  $\vec{q}_A = (q_i, q_j)$  in Eq 2.9  $\tilde{\Phi}(\vec{q}_B, \vec{q}_A)$ , respectively. The spatial correlation we seek to observe. When taking a Two-photon imaging we already deduce in the previous Chapter

that the image is going to be related with  $R(\vec{r}_A)$  from Eq. 2.23, where the  $(i_A, j_A)$  position is related with  $\vec{r}_A = (x_i, y_j)$ .

### 3.2.2 Single Photon Counting Module(SPCM)

Light is transmitted through an optic fiber from the pin hole detector to the SPCM. This consists in a self-contained module that detects single photons of light over the  $400\text{nm}$  to  $1069\text{nm}$  wavelength range. The module used is SPCM-AQRH-13, and it uses a unique silicon avalanche photodiode (SLiK) with a detection efficiency of more than 65%[17]. The result signal coming from the SPCM are pulses where each one represents one photon.



FIGURE 3.8: Single Photon Counting Module

### 3.2.3 Field-programmable gate array(FPGA)

Both  $A$  and  $B$  pulses from the respective SPCM goes to the same Field-Programmable Gate Array (FPGA). This FPGA (ZestSC1) is programmed to count the photon coincidences, this means that the FPGA is fast enough to detect and separate pulses from photons that are time-separated.

### 3.2.4 Computer(Data Analysis)

LabVIEW is used to control the detection module, and also, to receive and translate the information from the FPGA. It delivers the single and coincidence counts for every position in the scan grid, Fig. 3.7. Using this information is only a matter of using any way to handle this data and generate the graph for single and coincidence counts. Through this monograph it has been used the python language and the matplotlib library to generate them.

### 3.3 Two-Photon Imaging Setup

Figure 3.9 shows the extra parts of the experimental setup for doing Two-photon imaging. In path B we add an object and a bucket detector  $D_C$ . It may be noted that all the setups shown so far, use in essence the same optical elements. It is important to create an experimental setup that allows us to measure different things without changing it too much. For this we re-direct the light that goes through the object by means of a flip mirror (FM).

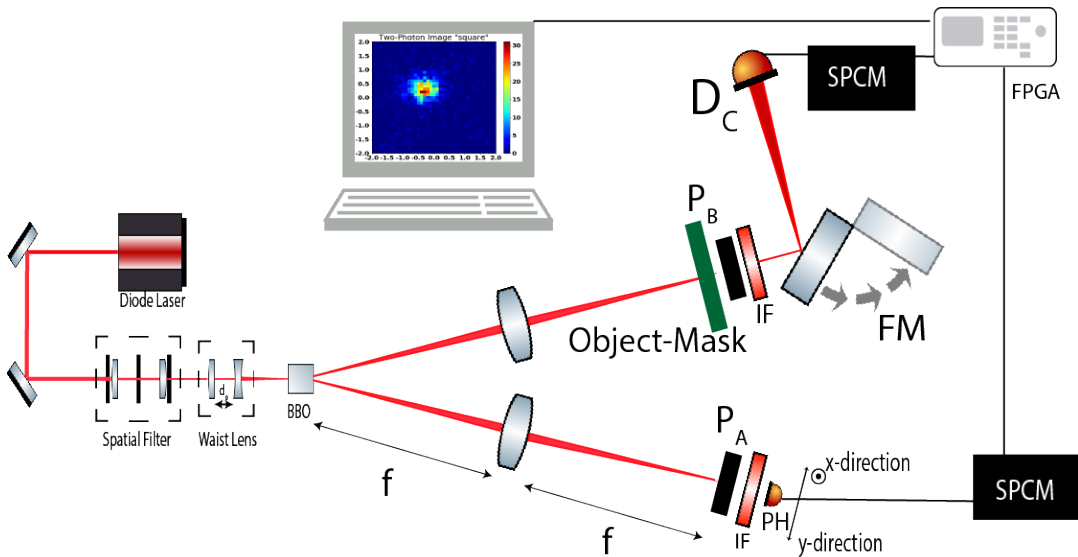


FIGURE 3.9: Experimental Setup for the Two-photon Imaging

The object is an obstruction that is placed in the  $B$  path. This is the object from which we will make an image. It consists on an aperture  $T(r_B)$  on a translational mount, that allow us to move the aperture precisely in the same plane we make our detections. This is done by manipulating a pair of screws. We used different objects and in Figure 3.10 there is a detailed schematic of the first one used. It consists on a square aperture placed in the 4th quadrant of the scanned plane.

In Figure 3.11 there are the other two apertures that we used so far in the experiment, these apertures were selected because of the symmetries and antisymmetries they present, and therefore they help us to recognise the effects of the spatial correlations in the image recovered.

In order to change the path followed by the B-photon, and guide the light to a new detector  $D_C$ , we use a Folding mirror. This mirror plays the role of a switch, when it is up, we are now dealing with the  $D_C$  detector, and we are doing a Two-photon Imaging process. In contrast, when the mirror is down,

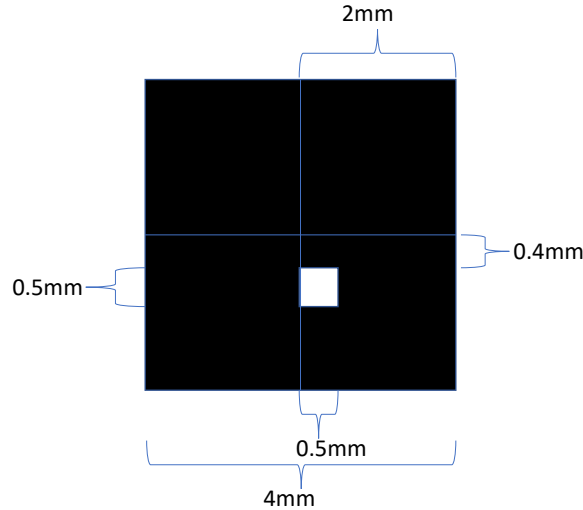


FIGURE 3.10: Mask 1: Detailed description of the 'square' aperture location in the scanned plane

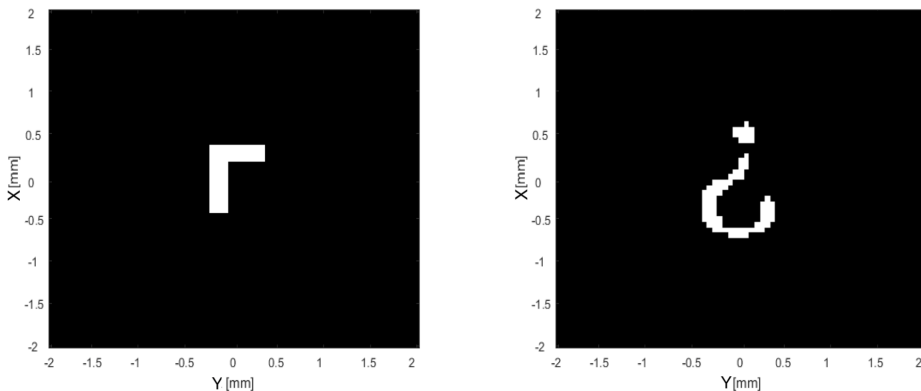


FIGURE 3.11: Mask 2: The letter 'L' pointing down. Mask 3: Opening question mark.

we are recovering spatial information, so it is possible to recognise some sort of shadow from the object, or to measure the spatial correlations.

The bucket detector  $D_C$  consists in a coupling lens, a multimode fiber and a detector. The lens collects all the light that goes through the object couple it to the fiber that is connected to the SPCM. In contrast to the other detections made before with  $D_A$  and  $D_B$ , the Bucket detector loses track of any spatial information of the photons.

# Chapter 4

## Results

In this chapter, we present the experimental data recovered through the different steps described in the Chapter before. Most the following results consists in 2-D arrays representing a matrix, where in each position a color is painted, depending on how many photons were detected in single or coincidences counts. As we have seen, before making a Two-photon image, there are some process that have to be made. The first thing to do is to achieve a Gaussian behavior of the original diode laser. For doing so, we have to look at the beam propagation after the Spatial Filter.

### 4.1 Achiiving a Gaussian Beam

From Eq. 3.1 we expect that the pump waist doesn't change too much with the distance traveled, for this reason we started by measuring the spatial profile of our pump beam in different distances from the spatial filter. Figure 4.1 shows the behaviour of the waist while we move away from the spatial filter. From the Figure we can observe that the waist doesn't change significantly, if we take a closer look in the x-axis, the total separation from the spatial filter ( $\sim 100\text{cm}$ ) its considerably bigger than the little change in the pump waist( $\sim 100\mu\text{m}$ ). There are 3 different lines in both Figures, the blue one corresponds to the pump waist at the 13.5% of the intensity, the red one to the 50% and the green one to the 80%.

Figure 4.2 shows the waist measured in the V and W direction, this waist correspond to the 13.5% of intensity. Using 3.1 we can make a fit to the experimental data. We observe that in the V direction the behaviour is closer to the one expected by theory for a gaussian beam, the blue line shows how the pump waist should change for a gaussian beam with origin point at  $z=0$ .

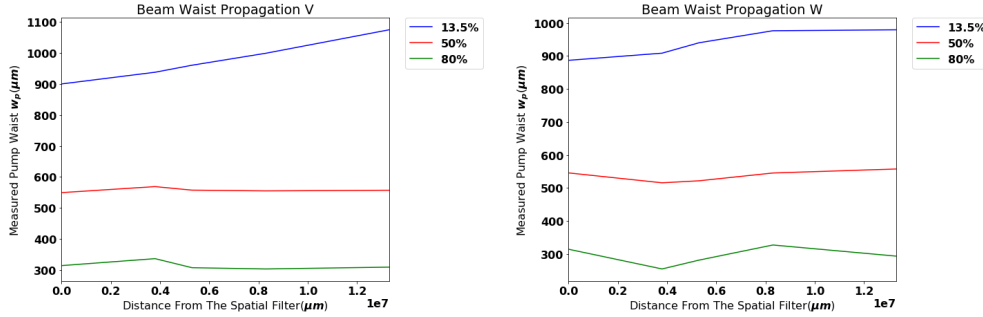


FIGURE 4.1: Propagation of the pump Beam, the graph shows how the  $w_p$  changes with distance

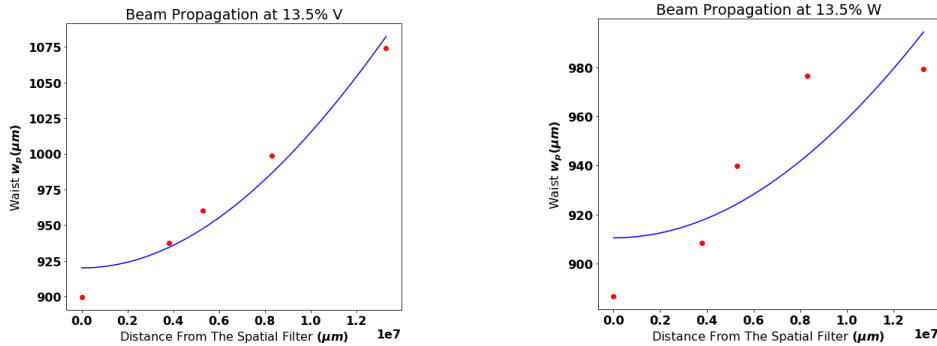


FIGURE 4.2: Fit for the change in the  $w_p$  with distance, at 13.5% intensity

## 4.2 Finding The Correlated Photons

After obtaining a Gaussian propagation, and measuring waist that no varies to much while propagates, we focused the laser at the BBO crystal and with the help of the *waist lens* we set the  $w_p = 91\mu m$ . Before observing the spatial correlations of the down converted photons, we make sure we are seeing them. Figure 4.3 shows two different images recovered, where in Fig.4.3(a) we found out that there is some problems with the alignment of the optical elements.

In Figure 4.3(b) we can see the B-photon, and now there is no interference caused by the bad alignment. As said before we placed a pair of polarisers in order to filter them. In the figure we can see that just one direction of the down converted pair of photons, while the other is partially filtered.

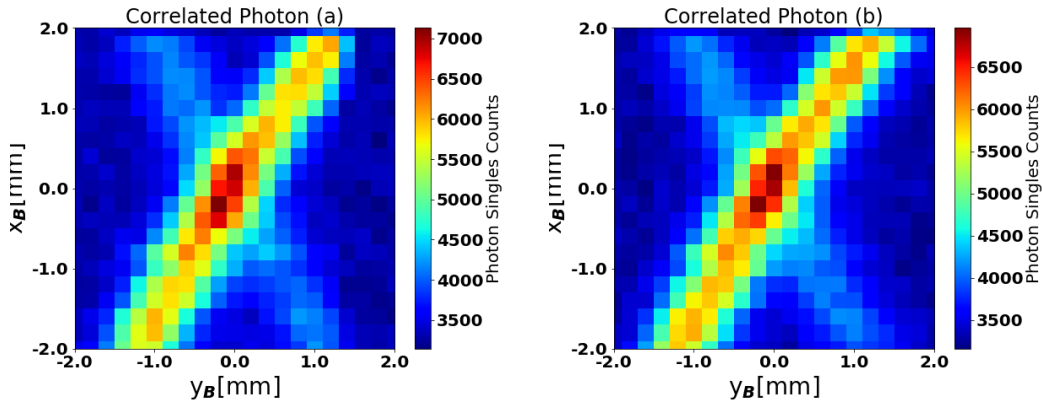


FIGURE 4.3: (a) and (b) shows the B-photon of the down converted pair. In (b) we moved away the translational mount of the mask

### 4.3 Experimental Correlations

After being sure of observing the correlated photons, we would like to observe the shape of the spatial correlations the pair of down converted photons and see the experimental behaviour of  $|\tilde{\Phi}(\vec{q}_B, \vec{q}_A)|$ . When remembering the definition of  $\vec{q}_n$ , it is a 2-D vector, containing the information of the photon in x and y direction. It is clear that when counting the two photons, we have 4 different correlations for the pair of photons, in this monograph we focus on the correlations on the type XX and YY. There is important to point out that this transverse momentum  $\vec{q}_n$  is related with his equivalent  $\vec{r}_n$  the position of the photon, with n making reference to the A and B paths.

In Figure 4.4 there are the correlations in the xx and yy direction. The 2-D matrix in Figure 4.4(XX Correlation) is the result of repeating this recipe: placing the  $D_A$  at a fixed position and scanning the  $D_B$  just in the x direction, next we move de  $D_A$  one position in the x direction. Repeating this N times we construct an image of the coincidence counts between  $D_A$  and  $D_B$  in every position.

Figure 4.4(YY Correlation) show the spatial correlation in the yy direction, this image is done by repeating the same recipe as before, but this time scanning and moving in the y direction. The spatial correlations in this case present a negative behaviour in both XX and YY direction, an anticorrelation. Meaning that is expected to measure a photon at a negative position at the B path if we measured a photon at a positive position at the A path. They both exhibit a elliptical shape, but the XX correlation is a narrower one, meaning there is a stronger relation between the pair of photons in the X direction.

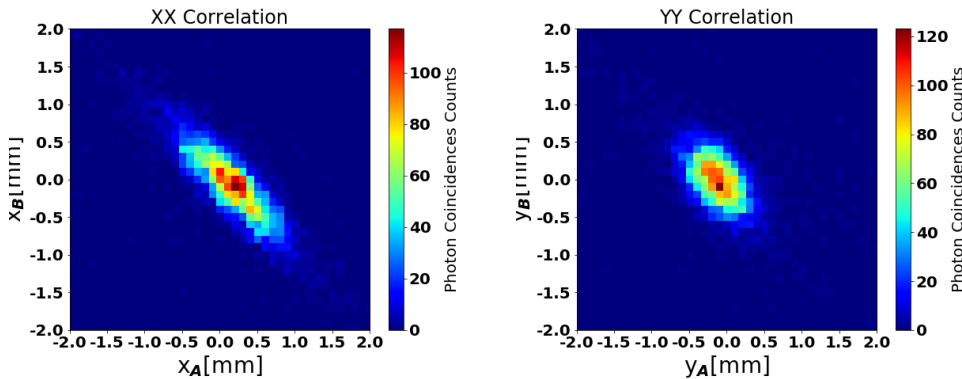


FIGURE 4.4: Experimental Spatial correlations between a pair of down-converted photons. *XX Correlation* shows the correlation in the x variables. *YY Correlation* shows the correlation in the y variables, Beam propagating in the z direction.

$$w_p = 91\mu m$$

## 4.4 Mask Alignment

Before making a Two-photon image we need to know that we have placed the mask in the correct spot. This correct spot is defined by the Figures 3.10 and 3.11. Which localisation was decided in function of where the flux of correlated photon was greater. The following images were produced as the standar image is done. It means we show the shadow of the aperture in the B path. Every position of the images is the single counts of the  $D_B$  in the exposure time.

### 4.4.1 Alignment Mask 1

The Following Figure 4.5 shows the final localisation of the first mask used. It was the final position because its position is really similar to the one described in Figure 3.10. For making this image we set the step length to be  $0.2mm$  and the exposure time was 1 second per position.

### 4.4.2 Alignment Mask 2

Figure 4.6 shows the localisation of the second mask. While in Figure 4.6(A) there is the initial position of the mask, Figure 4.6(B) shows the new localisation of the aperture after a translation in the y direction. This images were done by setting the steps to  $0.2mm$  and the exposure time to 1 second per position.

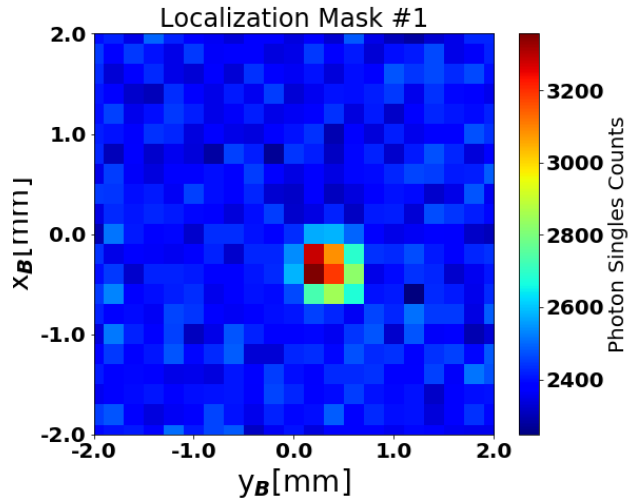


FIGURE 4.5: Localization of the mask with an square

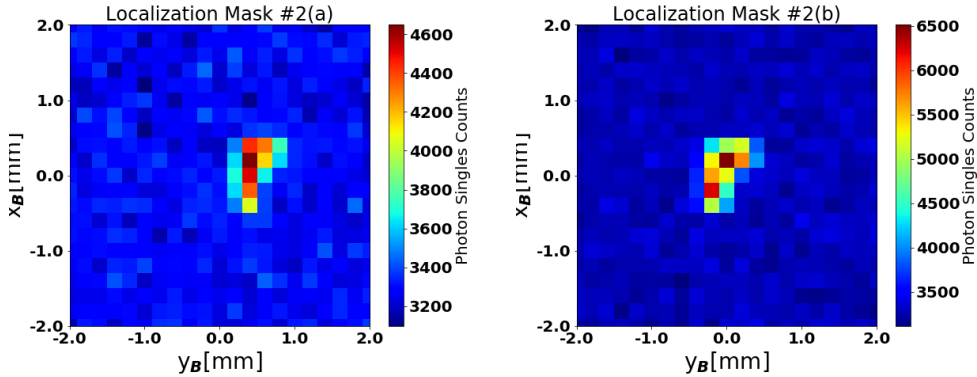


FIGURE 4.6: Moving the L Mask in order to put it in the most central spot

In Figure 4.7 is presented the definitive position of the aperture before making a Two-photon imaging. If we take a closer look to the Figure, we can appreciate a higher contrast, this is because in this opportunity we set the steps to be  $0.1\text{mm}$  and the exposure time to be 30 seconds per position. This image is the result of measuring for around 14 hours.

#### 4.4.3 Alignment Mask 3

The definitive localisation of the third mask used is presented in the Figure 4.8, where the step was  $0.1\text{mm}$  and the exposure time was set to 30 seconds per position.

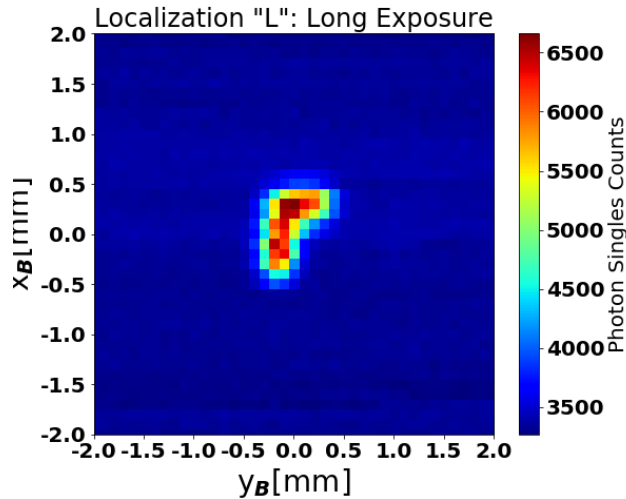


FIGURE 4.7: Long exposure of the definitive localization of the mask, in this try we leave the detector in each place for 30 seconds, we also make the steps of the detector smaller,  $0.1\text{mm}$

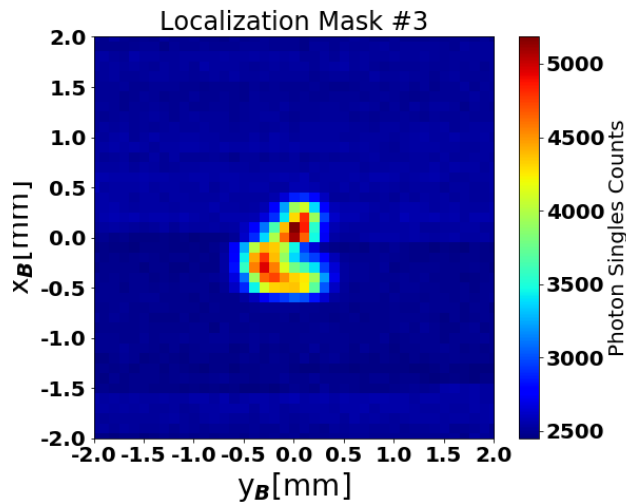


FIGURE 4.8: Interrogation definitive position

## 4.5 Two-Photon Images

Finally we get to observe the Two-photon images that are the core of this monograph. It is important to remember the way these images are obtained. The image  $R(\vec{r}_A)$  is a function of the coincidence counts between  $D_C$  and  $D_A$ . We scan  $D_A$ , and as a result we obtain a 2-D matrix where each  $(i, j)$  position is the coincidence counts.

### 4.5.1 Two-photon imaging Mask 1

Figure 4.9 is the Two-photon image of the square aperture. The maximum coincidence counts changed position in the image, compared to Figure 4.5. The shape is not identifiable, and its position is reflected in both x and y direction, as an evidence of the anticorrelations we are using Figure 4.4

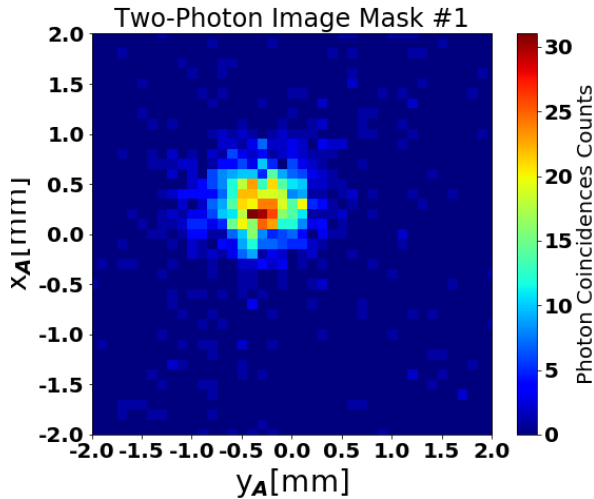


FIGURE 4.9: Experimental Two-photon image recovered for the square aperture

### 4.5.2 Two-photon imaging Mask 2

The Two-photon image of the second mask is presented in Figure 4.10. In this opportunity it is clear that the more complex shape of the aperture is hardly identifiable. However, there are some other interesting things to note about the image. As the original aperture, the image is not symmetrical, and it is not pointing to the original direction the L was in Figure ???. This make us to think about reflexions in the image respect from the original mask, but in this case is not that easy to detect.

### 4.5.3 Two-photon imaging Mask 3

The third Two-photon image is in Figure 4.11. Again the complex original shape is barely visible in the image obtained, Nevertheless this result and the other Two-photon image is really instructive about what we can expect with different spatial correlations. The step for this Figure was  $0.01\text{mm}$  and the exposure time was of 30 seconds per position.

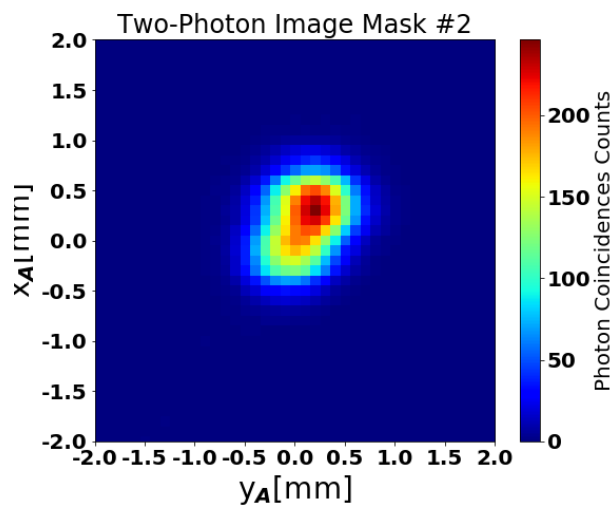


FIGURE 4.10: Two-photon image recovered for the L aperture.

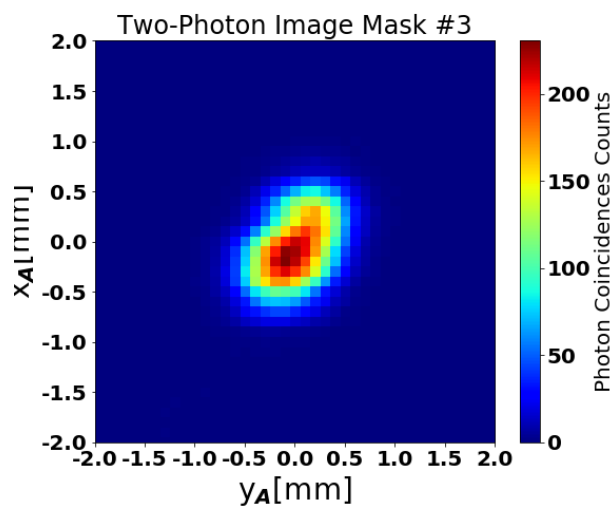


FIGURE 4.11: Two-Photon Image Interrogation

## Chapter 5

# Discussions and Conclusion

We used a light source that generates pair of entangled photons, however, we broke this entanglement and traced out all the temporal information. Still we were able to recover some of the characteristics of the objects used, this is an evidence of the capabilities of this source light. SPDC is an simple experimental process with not too many technical problems that is capable of producing pair of photons that can exhibit a strong correlation.

We presented an alternative technique to the problem presented at the introduction of this monograph. If we lose the ability to recover the spatial information of the reflected or scattered light from an object, we described along this work why Two-photon imaging can be an alternative. We can light the object with an strongly correlated light, and measure coincidences at a separated detector, and we may recover the image.

The Imaging process shared characteristics in both standard and Two-photon imaging versions. As discussed through this work and in Appendix A, The image recovered in coincidence counts, is a convolution between the transfer function  $T(\vec{r}_o)$  of the object, and a Second order correlations function  $G^{(2)}(\vec{r}_B, \vec{r}_A)$ . Meanwhile, in the standard imaging process we find out that the image recovered is a convolution between  $T(\vec{r}_o)$  and Sombrero-like function, which acts like the 'correlation' function between the light at the object and at the image.

The results presented so far are not completely exempt, the numerical simulations and the experimental data have points in common. In the numerical simulations the images suffered reflections about the axis in which the correlations was negative. In the experimental Two-photon imaging of the Mask 1, Fig. 4.9, the image was flipped in both directions, this was the expected behaviour that is present in the numerical solution.

It is clear that in order to achieve a higher spatial resolution we need to move to a regime where the spatial correlations are stronger, meaning that

they are elipsis more narrower, similar to straight lines. Wanting this narrow spatial correlations is equivalent to have a Sombrero-like function with a narrower point-spread function in the frame of standar imaging.

This Experimental procedure described through this monograph is the sum of many previous work, all the things done before were necessary to get to this point were the experiment is. It is a shame the time stipulated for a monograph is so short, the results presented so far, are just the first ones. To make an complete study of the phenomena of Two-photon using tuneable Spatial Correlations it is necessary to change the pump waist, in order to change the shape of spatial correlations.

## Appendix A

# Two-photon Imaging Using Chaotic Sources

In principle the term "thermal radiation" should refer only to radiation coming from a blackbody in thermal equilibrium at some temperature T. But with this realisation of thermal radiation we have to face some characteristics of true thermal fields. Thermal radiation is also referred as chaotic light, which have extreme short coherence time. This is because a thermal source contains a large number of independent sub-sources, such as the trillions of atoms or molecules. These atomic transitions that can be identical or different act like sub-sources, that emit light into independently and randomly.

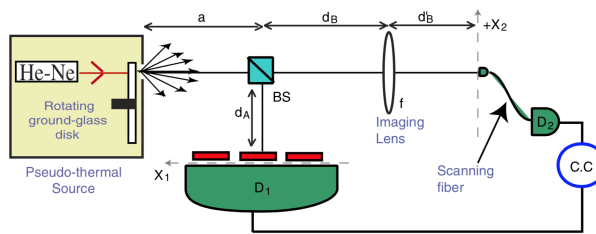


FIGURE A.1: Experimental setup for the Two-photon imaging using thermal light, taken from [6]

The source light in Figure A.1 is the one developed by Martinssen and Spiller[18] which is the most commonly used among the pseudothermal fields. A coherent laser radiation is focused on a rotating ground glass disk, the scattered radiation is chaotic with a Gaussian spectrum. After this, a nonpolarizing beam splitter (BS) splits the radiation in two distinct optical paths. In the reflected arm an object, with transmission function  $T(r_1)$ , is placed at a distance  $d_A$  from the BS and a bucket detector ( $D_1$ ) is just behind the object. In the transmitted arm an imaging lens, with focal length  $f$ , is placed at a distance  $d_B$  from the BS, and a multimode optical fiber ( $D_2$ ) scans the transverse plane at a distance  $d'_B$  from the lens. The output pulses from the two single

photon counters are sent to an electronic coincidence circuit to measure the rate of coincidence counts.

Once again we expect the joint-detection counting rate between photodetectors  $D_1$  and  $D_2$  to behave like the one described in Eq. 2.14. But this rate this coincidence counts is governed by the second-order Glauber correlation function [19]:

$$G^{(2)}(\vec{r}_1; \vec{r}_2) \equiv \langle E_1^{(-)}(\vec{r}_1) E_2^{(-)}(\vec{r}_2) \times E_2^{(+)}(\vec{r}_2) E_1^{(+)}(\vec{r}_1) \rangle \quad (\text{A.1})$$

where the  $E^{(-)}$  and  $E^{(+)}$  are the negative-frequency and the positive-frequency field operators describing the detection events at the locations  $\vec{r}_1$  and  $\vec{r}_2$ . The transverse second-order correlation function for a thermal source is given by [6]:

$$G_{\text{thermal}}^{(2)}(\vec{r}_1; \vec{r}_2) \propto \sum_{\vec{q}} |g_1(\vec{q}, \vec{r}_1)|^2 \sum_{\vec{q}'} |g_2(\vec{q}', \vec{r}_2)|^2 + |\sum_{\vec{q}} g_1^*(\vec{q}, \vec{r}_1) g_2(\vec{q}, \vec{r}_2)|^2 \quad (\text{A.2})$$

where  $\vec{r}_i$  is the transverse position of the detector  $D_i$ ,  $\vec{q}$  and  $\vec{q}'$  are the transverse components of the momentum vectors, and  $g_i(\vec{q}, \vec{r}_i)$  is the Green's function associated with the propagations of the field with transverse momentum  $\vec{q}$  from the source, to the position  $\vec{r}_i$  at the detection plane defined by the detector  $D_i$ .  $g_i(\vec{q}, \vec{r}_i)$  is defined in a similar way as in Eq. 2.17.

It is important to note that there are two main differences with respect to the SPDC case: First the presence of a background noise (first term of Eq. A.2), which does not exist for SPDC. Second, the possibility of writing the second term of Eq. A.2 as a product of the first order correlation functions,  $G_{12}^{(1)} G_{21}^{(1)}$ , while there is no way to write the biphoton produced by the SPDC as a product of other correlations. Also this term  $|\sum_{\vec{q}} g_1^*(\vec{q}, \vec{r}_1) g_2(\vec{q}, \vec{r}_2)|^2$  Is the interference of intensities of a incoherent statistical ensemble of randomly distributed photons.

Following the process done in [6], it can be shown that for any values of distances  $d_A$ ,  $d_B$  and  $d'_B$  which obey the equation:

$$\frac{1}{d_B - d_A} + \frac{1}{d'_B} = \frac{1}{f} \quad (\text{A.3})$$

which clearly has the form on a thin-lens equation, defining a point-to-point correspondence between imaging and object plane. Then Eq. A.2 can be simplified as:

$$G_{\text{tot}}^{(2)}(\vec{r}_2) \propto N + |T \left( \frac{d_A - d_B}{d'_B} \vec{r}_2 \right)|^2 \quad (\text{A.4})$$

where  $T(\frac{d_A - d_B}{d_B} \vec{r}_2)$  is the object transmission function ( $T(\vec{r}_1)$ ) reproduced on the  $D_2$  plane. Thanks to this result we can conclude that a thermal source allows reproducing in coincidence measurements the two-photon image of an object, similarly to the SPDC case, except for a constant background noise, where  $N$  is proportional to it.

It is possible to establish an analogy between classical optics and entangled two-photon optics: the two-photon probability amplitude plays in entangled two-photon processes the same role that the complex amplitude of the electric field plays in classical optics [6].

# Bibliography

- [1] T B. Pittman, Yanhua Shih, D V. Strekalov, and Alexander Sergienko. Optical imaging by means of two-photon quantum entanglement. *Physical review. A*, 52:R3429–R3432, 12 1995.
- [2] Omar Calderón-Losada, Jefferson Flórez, Juan P. Villabona-Monsalve, and Alejandra Valencia. Measuring different types of transverse momentum correlations in the biphoton's fourier plane. *Opt. Lett.*, 41(6):1165–1168, Mar 2016.
- [3] Jeffrey H. Shapiro and Robert W. Boyd. The physics of ghost imaging. *Quantum Information Processing*, 11(4):949–993, Aug 2012.
- [4] Inc. Thorlabs. Thorlabs, inc. <https://www.thorlabs.com/index.cfm>. Accessed: 2018-03-09.
- [5] E. Hecht. *Optics*. Pearson education. Addison-Wesley, 2016.
- [6] Alejandra Valencia, Giuliano Scarcelli, Milena D'Angelo, and Yanhua Shih. Two-photon imaging with thermal light. *Phys. Rev. Lett.*, 94:063601, Feb 2005.
- [7] Giuliano Scarcelli, Alejandra Valencia, and Yanhua Shih. Experimental study of the momentum correlation of a pseudo-thermal field in the photon counting regime. *Conference on Lasers and Electro-Optics/Quantum Electronics and Laser Science and Photonic Applications Systems Technologies*, page JTuC122, 2005.
- [8] MaLin Zhong, Ping Xu, LiangLiang Lu, and ShiNing Zhu. Resolution of ghost imaging with entangled photons for different types of momentum correlation. *Science China Physics, Mechanics & Astronomy*, 59(7):670311, May 2016.
- [9] Lorenzo Basano and Pasquale Ottomello. Experiment in lensless ghost imaging with thermal light. *Applied Physics Letters*, 89(9):091109, 2006.

- [10] A. Einstein, B. Podolsky, and N. Rosen. Can quantum-mechanical description of physical reality be considered complete? *Phys. Rev.*, 47:777–780, May 1935.
- [11] Clara I Osorio, Alejandra Valencia, and Juan P Torres. Spatiotemporal correlations in entangled photons generated by spontaneous parametric down conversion. *New Journal of Physics*, 10(11):113012, 2008.
- [12] Jefferson Flórez, Omar Calderón, Alejandra Valencia, and Clara I. Osorio. Correlation control for pure and efficiently generated heralded single photons. *Phys. Rev. A*, 91:013819, Jan 2015.
- [13] Y. Shih. *An Introduction to Quantum Optics: Photon and Biphoto Physics*. Series in Optics and Optoelectronics. Taylor & Francis, 2011.
- [14] Morton H. Rubin. Transverse correlation in optical spontaneous parametric down-conversion. *Phys. Rev. A*, 54:5349–5360, Dec 1996.
- [15] Miguel A. Bandres and Julio C. Gutiérrez-Vega. Ince–gaussian beams. *Opt. Lett.*, 29(2):144–146, Jan 2004.
- [16] D. N. Nikogosyan. Beta barium borate (bbo). *Applied Physics A*, 52(6):359–368, Jun 1991.
- [17] PerkinElmer. *Single Photon Counting Modules – SPCM*, 2010. Rev. 1.
- [18] W. Martienssen and E. Spiller. Coherence and fluctuations in light beams. *American Journal of Physics*, 32(12):919–926, 1964.
- [19] Roy J. Glauber. The quantum theory of optical coherence. *Phys. Rev.*, 130:2529–2539, Jun 1963.